

1 Chronostratigraphic framework and provenance of the 2 Ossa-Morena Zone Carboniferous basins (SW Iberia)

3
4 Manuel Francisco Pereira^{1*}, Cristina Gama¹, Ícaro Dias da Silva I.², José Brandão
5 Silva³, Mandy Hofmann⁴, Ulf Linnemann⁴, Andreas Gärtner⁴

6 1- Instituto de Ciências da Terra, Departamento de Geociências, ECT, Universidade de Évora, Apt.94,
7 7002-554 Évora, Portugal

8 2- Instituto Dom Luiz, Faculdade de Ciências da Universidade de Lisboa, Campo Grande, 1749-016
9 Lisboa, Portugal

10 3- Instituto Dom Luiz, Departamento de Geologia, Faculdade de Ciências da Universidade de Lisboa,
11 Campo Grande, 1749-016 Lisboa, Portugal

12 4- Senckenberg Naturhistorische Sammlungen Dresden, Museum für Mineralogie und Geologie,
13 Germany

14
15 Correspondence to: M. Francisco Pereira (mpereira@uevora.pt)

16
17 **Abstract.** Carboniferous siliciclastic and silicic magmatic rocks from the Santa Susana-São
18 Cristovão and Cabrela regions contain valuable information regarding the timing of synorogenic
19 processes in SW Iberia. In this region of the Ossa-Morena Zone (OMZ), Late Carboniferous
20 terrigenous strata (i.e. the Santa Susana Formation) unconformably overlie Early Carboniferous
21 marine siliciclastic deposits alternating with volcanic rocks (i.e. the Toca da Moura volcano-
22 sedimentary complex). Lying below this intra-Carboniferous unconformity, the Toca da Moura
23 volcano-sedimentary complex is intruded and overlain by the Baleizão porphyry. Original
24 SHRIMP and LA-ICP-MS U-Pb zircon are presented in this paper, providing
25 chronostratigraphic and provenance constraints, since available geochronological information is
26 scarce and only biostratigraphic ages are currently available for the Santa Susana-São Cristovão
27 region. Our findings and the currently-available detrital zircon ages from Paleozoic terranes of
28 SW Iberia (Pulo do Lobo Zone- PLZ, South-Portuguese Zone- SPZ, and OMZ), were jointly
29 analyzed using the K-S test and MDS diagrams to investigate provenance. The marine
30 deposition is constrained to the age interval of c. 335-331 Ma (Visean) by new U-Pb data for
31 silicic tuffs from the Toca da Moura and Cabrela volcano-sedimentary complexes. The Baleizão
32 porphyry, intrusive in the Toca da Moura volcano-sedimentary complex, yielded a
33 crystallization age of c. 318 Ma (Bashkirian), providing the minimum age for the overlying
34 intra-Carboniferous unconformity. A comparison of detrital zircon populations from siliciclastic
35 rocks of the Cabrela and Toca de Moura volcano-sedimentary complexes of the OMZ suggests

36 that they derived from distinct sources more closely associated with the SPZ and PLZ than the
37 OMZ. Above the intra-Carboniferous unconformity, the Santa Susana Formation is either the
38 result of the recycling of distinct sources located in the Laurussian-side (SPZ and PLZ) and
39 Gondwanan-side (OMZ) of the Rheic suture zone. The best estimate of the crystallization age of
40 a granite cobble found in a conglomerate from the Santa Susana Formation yielded c. 303 Ma
41 (Kasimovian-Gzhelian), representing the maximum depositional age for the terrestrial strata.
42 The intra-Carboniferous unconformity seems to represent a stratigraphic gap of approximately
43 12-14 Ma, providing evidence of the rapid post-accretion/collision uplift of the Variscan
44 orogenic belt in SW Iberia (i.e. the OMZ, PLZ and SPZ).

45

46 **1. Introduction**

47 The Variscan orogen that extends from central Europe to Iberia was reworked through discrete
48 Carboniferous sedimentary cycles during the Laurussia-Gondwana convergence, giving rise to
49 the formation of marine and terrestrial basins. In SW Iberia, stratigraphic correlation has been
50 proposed for the Carboniferous synorogenic strata found in the three main tectonostratigraphic
51 divisions of the Variscan Orogen: the Ossa-Morena (OMZ), Pulo do Lobo (PLZ) and South
52 Portuguese (SPZ) zones (Quesada and Oliveira, 2019, and references therein).

53 The Carboniferous siliciclastic strata in the Santa Susana-São Cristovão and Cabrela regions
54 (OMZ) includes fossils indicating Carboniferous to Kasimovian biostratigraphic ages (Teixeira,
55 1938-1940, 1941; Lemos de Sousa and Wagner, 1983; Wagner and Lemos de Sousa, 1983;
56 Pereira et al., 2006; Machado et al., 2012; Lopes et al., 2014). In the Santa Susana-São
57 Cristovão region, Late Carboniferous siliciclastic strata of the Santa Susana Formation
58 unconformably overlie: i) the Baleizão volcanic-subvolcanic suite that was previously dated
59 with whole-rock Rb-Sr isochrons (Priem et al., 1986), and ii) the early Carboniferous Toca da
60 Moura volcano-sedimentary complex, which includes volcanic rocks that have never been
61 dated. This intra-Carboniferous unconformity was generated as consequence of regional uplift
62 and falling sea level, leading to a change in depositional environment from Early Carboniferous
63 marine to Late Carboniferous terrestrial (Gonçalves and Carvalhosa, 1984; Oliveira et al., 1991;
64 Machado et al., 2012). The provenance of the above-mentioned Carboniferous strata has been
65 discussed based on petrographic, paleontological and detrital zircon geochronology evidence
66 (Pereira et al., 2006; Machado et al., 2012; Lopes et al., 2014; Dinis et al., 2018).

67 In this paper, SHRIMP and LA-ICP-MS U-Pb analyses were performed on zircon grains from
68 silicic volcanic, subvolcanic, and siliciclastic rocks sampled in the Santa Susana-São Cristovão
69 and Cabrela regions (OMZ, SW Iberia). The aim of this geochronology study is to establish the
70 chronostratigraphic framework of these Carboniferous strata and to discuss their provenance
71 using a statistical approach (Kolmogorov-Smirnov test and Mutiscaling diagrams). Thus we pay

72 tribute to J.R. Martínez-Catalán, who devoted part of his career to investigating the
73 Carboniferous synorogenic basins of NW Iberia.

74

75 **2. Geological setting**

76 In SW Iberia, the tectonic limit between the OMZ (Gondwanan-side) and the PLZ and SPZ
77 (Laurussian-side) has been regarded as constituting the tectonically reworked suture zone of the
78 Rheic Ocean (Andrade, 1983; Quesada et al., 1994; Simancas et al., 2005; Díaz-Apiroz et al.,
79 2006; Ribeiro et al., 2007; Pereira et al., 2017a) (Fig. 1). This Paleozoic suture zone has been
80 defined along the Beja-Acebuches ophiolitic complex (Fonseca et al., 1999, and references
81 therein). The Beja-Acebuches ophiolitic complex is separated from the Beja Igneous Complex
82 (Jesus et al., 2007, 2016) by a strike-slip fault. Metabasalts and metagabbros (i.e. the Mombeja
83 unit of Andrade, 1983) from the Beja-Acebuches ophiolitic complex have been dated at c. 340-
84 332 Ma (U-Pb zircon; Azor et al., 2008), while in the Beja Igneous Complex gabbro and
85 granitic rocks are relatively older, yielding crystallization ages of c. 353-342 Ma (U-Pb zircon;
86 Jesus et al., 2007; Pin et al., 2008). Trace element and isotopic signatures of Beja Igneous
87 Complex plutonic rocks indicate crustal contamination of parental magmas deriving from a
88 depleted asthenospheric mantle reservoir (Santos et al., 1990; Pin et al., 2008; Jesus et al.,
89 2016). The plutonic rocks of the Beja Igneous Complex show well-defined intrusive contacts
90 with previously deformed and metamorphosed sedimentary and igneous rocks of the OMZ
91 basement (Rosas et al., 2008; Pin et al., 2008). The Beja Igneous Complex also includes the São
92 Cristovão-Alcáçovas subvolcanic complex (Gonçalves and Carvalhosa, 1984), composed of
93 silicic sub-volcanic and volcanic rocks (i.e. the Baleizão unit of Andrade, 1983), granophyres
94 and porphyries dated at c. 319 Ma (whole-rock Rb-Sr isochrons; Priem et al., 1986), associated
95 with diabases. Porphyry dykes are found cutting across the OMZ basement that is here formed
96 by Cambrian igneous rocks with c. 527 Ma (Alcáçovas gneiss, Chichorro et al., 2008) deformed
97 and metamorphosed in the Early Carboniferous at 340 ± 6 Ma (Pereira et al., 2009). The major
98 and trace element geochemistry of the Baleizão porphyries indicates a calc-alkaline rhyolitic,
99 rhyodacitic and andesitic composition typical of magmas produced at convergent plate
100 boundaries (Santos et al., 1987; Caldeira et al., 2007; Ferreira et al., 2014). The Baleizão
101 porphyries occur as dykes and sills (Andrade, 1927) (Figs. 3a, b), overlying (Gonçalves and
102 Carvalhosa, 1984) the Early Carboniferous siliciclastic and volcanic rocks of the Toca da Moura
103 volcano-sedimentary complex (Santos et al., 1987, and references therein) (Fig. 2).
104 The Toca da Moura volcano-sedimentary complex is mainly composed of pelites (i.e.
105 “Xistinhos”; Teixeira, 1944; Fig. 3a) and greywackes, associated with andesite-to-rhyolite
106 volcanic rocks (lava flow and tuffs; Figs. 3c, d, e), andesitic basalt, chert layers (Gonçalves and
107 Carvalhosa, 1984), and a few olistoliths of basalt and limestone. Siliciclastic rocks contain well-
108 preserved in-situ palynomorph assemblages of Tournaisian to Viséan age and reworked

109 palynomorphs ranging in age from the Middle Cambrian to the Early Tournaisian (Pereira et al.,
110 2006; Lopes et al., 2014). Based on geochemical information, this volcanism was interpreted by
111 Santos et al. (1987) as deriving from calc-alkaline magma produced in a continental magmatic
112 arc. A stratigraphic correlation was established between the Toca da Moura volcano-
113 sedimentary complex and the Cabrela volcano-sedimentary complex (Pereira et al., 2006) which
114 is located 15 km to the NW, in the Évora Massif (Pereira et al., 2007; 2012a) (Fig. 1b). The
115 presence of variable-scale soft-sediment structures (i.e. slumps, intraclast conglomerates and
116 olistoliths) in both complexes indicates gravity-induced instability during marine sedimentation.
117 Detrital zircon ages of a siliciclastic rock from the Cabrela volcano-sedimentary complex
118 interbedded with silicic tuffs (Fig. 3f) are mainly Middle-Late Devonian (82%) and Early
119 Carboniferous (14%), also including a few older grains (sample OM-200 from Pereira et al.,
120 2012a).

121 The Santa Susana Formation (i.e. Santa Susana basin, Domingos et al., 1983; Quesada et al.,
122 1990, Oliveira et al. 1991) siliciclastic rocks that outcrop along a NNW-SSE-trending narrow
123 discontinuous band which is 0.1-5 km wide and 12 km long unconformably overlie the Baleizão
124 Porphyry and the Toca da Moura volcano-sedimentary complex (Fig. 2), forming the geological
125 contact between these stratigraphic units often defined by faults (Gonçalves and Carvalhosa,
126 1984). The Santa Susana Formation is divided into two members (Machado et al., 2012, and
127 references therein): i) the lower member is mainly composed of coarse-grained sandstone and
128 conglomerate beds (Figs. 4a, b, c, d); these conglomerates include pebbles and cobbles of silicic
129 porphyry, rhyolite, andesite, basalt, granite, felsic tuff, pelite, sandstone, greywacke, quartzite,
130 phyllite, chert, and quartz (Figs. 4e, f); ii) the upper member represents a repetitive sequence of
131 alternating beds of pelite and sandstone interbedded with coal seams, and few beds of
132 conglomerate (Fig. 2). These terrestrial deposits were most probably deposited in an
133 alluvial/fluviol-to-fluvial/lacustrine (floodplain lakes and/or abandoned channels with abundant
134 vegetation) system (Machado et al., 2012, and references therein). The plant fossils identified in
135 the siliciclastic rocks of the Santa Susana Formation indicate a Moscovian-Kasimovian
136 biostratigraphic age (Wagner and Lemos de Sousa, 1983). Pelitic beds from the Upper member
137 include palynomorph assemblages assigned with Kasimovian age (Machado et al., 2012).

138 Palynomorphs ranging in age from the middle Cambrian to the early Moscovian were also
139 found in siliciclastic rocks of the Santa Susana Formation sampled from a borehole at a depth of
140 around 400 m (Lopes et al., 2014). Detrital zircon ages from upper member sandstones (Dinis et
141 al., 2018) are mainly distributed over Devonian-Carboniferous (41-51%), Paleoproterozoic (23-
142 30%) and Ediacaran-Cryogenian (16-23%) groups, and also a few Stenian-Tonian and Archean
143 grains.

144

145 **3. Rational and analytical methods**

146 U-Pb geochronology of detrital zircon from siliciclastic rocks has been extensively used in
147 stratigraphic correlation studies for estimating the maximum depositional age and investigating
148 the provenance of sedimentary sequences (Fedo et al., 2001; Dickinson and Gehrels, 2009). The
149 youngest detrital zircon grains found in siliciclastic rock commonly provide useful information
150 about depositional age, especially in areas that experienced active volcanism during sediment
151 accumulation (Gehrels, 2014). The maximum depositional age obtained for siliciclastic rock is
152 often not necessarily coincident with the biostratigraphic age as defined by key fossil
153 assemblages (Pereira et al., 2019). Therefore, in order to overcome any doubt about the true age
154 of deposition, it is desirable that volcanic rocks interstratified with fossiliferous siliciclastic
155 rocks should be dated (Fedo et al., 2001; Bowring et al., 2006). Furthermore, the application of
156 zircon U-Pb geochronology to volcano-sedimentary and sedimentary sequences that are
157 separated by unconformities, by means of the comparative analysis of their age populations,
158 may be useful for estimating time intervals and revealing changes in provenance. Volcanic
159 rocks that lie beneath or overlie sedimentary sequences and unconformities can provide
160 maximum and minimum ages, respectively. When detrital zircon geochronology is linked to the
161 geochronology of crosscutting younger igneous rocks, then both a maximum and minimum age
162 bracket for deposition can be determined (Fedo et al., 2001).

163 In this study, SHRIMP U-Pb analyses were performed for the first time on magmatic zircon
164 from two tuffs from the Toca da Moura volcano-sedimentary complex (TM-1 and SCV-2; Figs.
165 3c, d), one tuff from the Cabrela volcano-sedimentary complex (CBR-12), one from the
166 Baleizão silicic porphyry (SCV-30; Fig. 3b), and a cobble of granite (SCV-7; Fig. 4e) found in a
167 conglomerate from the lower member of the Santa Susana Formation. Estimations of the
168 crystallization age of samples SCV-2, TM-1 and CBR-12 (syndepositional volcanism), and
169 sample SCV-30 (post-depositional) were used to validate the Tournaisian-Viséan
170 biostratigraphic age previously attributed to the Toca da Moura and Cabrela volcano-
171 sedimentary complexes based on palynological assemblages (Pereira et al., 2006; Lopes et al.,
172 2014). The presence of granite cobbles and pebbles in conglomerate layers from the lower Santa
173 Susana Formation indicates denudation and recycling of a crystalline basement involving
174 granite whose age is unknown. The dating of the granite cobble (sample SCV-7) is useful for
175 discussing provenance and estimating the maximum depositional age of the Santa Susana
176 conglomerate. In addition, LA-ICP-MS U-Pb analyses were performed on detrital zircon grains
177 from two samples of sandstone from the upper and lower members of the Santa Susana
178 Formation (samples SS-1 and SS-2, respectively; Fig. 5g, h), and a sample of pelite from the
179 Toca da Moura volcano-sedimentary complex (sample TM-3; Fig. 5e). This new U-Pb data is
180 useful for discussing provenance and determining the maximum depositional ages of the two
181 sedimentary sequences separated by an intra-Carboniferous unconformity. Sample locations in
182 the Santa Susana-São Cristovão region are indicated in Figure 2. Finally, detrital zircon grains

183 of siliciclastic rock from the Cabrela volcanic-sedimentary complex (sample CBR-11; Fig. 5f;
184 equivalent to sample OM-200 of Pereira et al. 2012a) were analyzed to test for the existence of
185 pre-Devonian ages. The new U-Pb results obtained in the present study are compared with
186 previously-reported age spectra for pre-Kasimovian siliciclastic rocks from the OMZ, PLZ and
187 SPZ siliciclastic sequences of SW Iberia, using statistical tools.

188 Zircon grains for U-Pb geochronology were selected using traditional techniques: density
189 separation using a wilfley table (Universidad Complutense de Madrid, Spain) and also using
190 granulometric separation using sieves with a mesh size of less than 500 microns, density
191 (panning) separation procedures, and mineral identification using a binocular lens and
192 preparation of epoxy resin mounts with zircon grains (Universidade de Évora, Portugal). U-Pb
193 measurements were obtained at IBERSIMS (Universidad de Granada, Spain) using SHRIMP,
194 and also at the Senckenberg Naturhistorische Sammlungen Dresden (Museum für Mineralogie
195 und Geologie, Germany) using a LA-ICP-MS. U-Pb measurements using SHRIMP and LA-
196 ICP-MS followed the procedures previously described by Dias da Silva et al. (2018) and Pereira
197 et al. (2012a), respectively. U-Pb results are listed in Tables S1 and S2 (Supplementary
198 Material). Concordia curves and weighted-average means were obtained using Isoplot 4
199 (Ludwig, 2003) (Figs. 6 and 7). Kernel density estimation (KDE) diagrams were produced with
200 90-110 % concordant $^{206}\text{Pb}/^{238}\text{U}$ ages for grains younger than 1.0 Ga, and $^{207}\text{Pb}/^{206}\text{Pb}$ ages for
201 older grains (for further details, see Frei and Gerdes, 2009) using IsoplotR (Vermeesch, 2018)
202 (Figs. 8a, b). Cathodoluminescence-imaging was performed at TU Bergakademie Freiberg
203 (Germany) and at IBERSIMS.

204 The K-S test and the MDS technique were used in conjunction to compare populations of
205 detrital zircon U-Pb ages obtained from the Carboniferous siliciclastic rocks of the Santa
206 Susana-São Cristovão region using a method designed for a recent study of the provenance of
207 Triassic sandstones (Gama et al., in press, and references therein). The K-S test is a non-
208 parametric statistical tool that has been successfully used for the comparison of two populations
209 of detrital zircon U-Pb ages by evaluating whether they are significantly different, i.e. indicating
210 whether zircon age populations correlate with a similar source or not, regardless of whether they
211 are of different sizes, while including at least 20 measurements (DeGraaff-Surpless et al., 2003).

212 The probability of the observed maximum vertical difference between the cumulative
213 probability curves (D-value) being unrelated to age differences between the two detrital zircon
214 populations is given by a P-value corresponding to a confidence interval of 95% (Barbeau Jr. et
215 al.; 2009; Guynn and Gehrels, 2010) (Fig. S1; supplementary material). High P-values and low
216 D-values indicate that the observed difference between the two detrital zircon populations may
217 be explained by the existence of common sources (Gama et al., 2020, and references therein).

218 K-S analyses were carried out using an Excel spreadsheet published on the University of
219 Arizona Geochronological Center website at

220 <https://sites.google.com/a/laserchron.org/laserchron/>. The MDS technique provides a means for
221 the comparison of samples based on quantified pairwise comparisons of their detrital zircon
222 ages, and is extremely useful for visualising the degree of similarity between samples in two
223 dimensions, i.e. greater distances between samples represent a greater degree of dissimilarity
224 between points on MDS diagrams (Vermeesch, 2013; Spencer and Kirkland, 2015; Wissink et
225 al., 2018) (Fig. 9). MDS diagrams were produced using IsoplotR (Vermeesch, 2018).

226

227 **4. U-Pb geochronology: Results**

228 **4.1. Volcanic silicic rocks of the Toca da Moura and Cabrela volcano-sedimentary**

229 **complexes**

230 Sample SCV-2 is a fine-grained banded rhyolitic tuff consisting of variable size and shape
231 quartz and K-feldspar phenocrysts and lithoclasts (less than 1mm in diameter) dispersed in ash
232 matrix (Fig. 5a). Zircon grains appear as stubby-to-elongated euhedral prisms (50-150 μm in
233 diameter), mostly showing oscillatory concentric zoning growing on distinct cores or as simple
234 crystals. There are some dark inclusions, unzoned patches and transgressive variably
235 luminescence embayments. A total of 44 U-Th-Pb SHRIMP analyses of 44 grains yielded U
236 content ranging from 262 to 628 ppm. A group of 23 grains with $^{206}\text{Pb}/^{238}\text{U}$ ages (discordance \leq
237 5%) yielded a weighted mean $^{208}\text{Pb}/^{238}\text{U}$ age of 331 ± 4 Ma (MSWD = 1.2; Fig. 6a), which
238 probably represents the crystallization age of tuff.

239 Sample TM-1 is a fine-grained banded rhyolitic tuff consisting quartz, K-feldspar and biotite
240 phenocrysts, flattened dark-brown pumice (i.e. fiamme) and lithoclasts (less than 1mm in
241 diameter) enclosed in ash matrix (Fig. 5b). The zircon population is characterized by stubby
242 euhedral-to-sub-euhedral small (30-100 μm in diameter) grains. Magmatic grains are either
243 simple with concentric zoning or composite showing variably luminescence cores with
244 concentric zoning, unzoned, or banded zoned. These cores are surrounded by overgrowths with
245 concentric zoning and are occasionally diffuse or unzoned. A total of 120 U-Th-Pb LA-ICP-MS
246 analyses yielded U content ranging from 87 to 4136 ppm. 28 $^{206}\text{Pb}/^{238}\text{U}$ ages (90-110% of
247 concordance) yield a weighted mean $^{208}\text{Pb}/^{238}\text{U}$ age of 341 ± 10 Ma with a very poor fit (MSWD
248 = 6.9; Fig. 6b), as indicated by the scattering of ages along the Concordia curve. A coherent
249 group of 21 grains with $^{206}\text{Pb}/^{238}\text{U}$ ages yielded a weighted mean $^{208}\text{Pb}/^{238}\text{U}$ age of 335 ± 6 Ma
250 (MSWD = 1.5; Fig. 6b), providing the best age estimate for the volcanic rock (Fig. 6b). The
251 youngest zircon grain (c. 302 Ma) probably experienced Pb loss. The six oldest zircon grains
252 present Paleoproterozoic (c. 2 Ga), Neoproterozoic (c. 715 Ma) and Devonian (c. 395-378 Ma)
253 ages, suggesting inheritance.

254 Sample CBR-12 is a fine-grained rhyolitic rock in which feldspar and quartz phenocrysts and
255 lithic fragments occur embedded in altered very-fine grained matrix of quartz, sericite and
256 chlorite, including devitrified shards. Zircon (40-150 μm in diameter) appears as stubby-to-

257 elongated euhedral prisms, mostly showing oscillatory concentric zoning, sometimes disturbed
258 by inclusions, as simple grains or as overgrowths. A few crystals show banded zoning or are
259 diffuse or unzoned. Thirty-two analyses were performed on this silicic volcanic rock yielding U
260 content ranging from 288 to 2587 ppm. Twenty-two analyses with discordance $\leq 5\%$, yielded a
261 weighted mean $^{208}\text{Pb}/^{238}\text{Th}$ age of 335 ± 2 Ma (MSWD = 1.2; Fig. 6c). The oldest two grains
262 yielding $^{206}\text{Pb}/^{238}\text{U}$ ages of c. 389 and 371 Ma are interpreted to represent xenocrysts.

263

264 **4.2. Baleizão porphyry**

265 Sample SCV-30 is a porphyritic rhyodacite-rhyolite consisting of quartz, plagioclase, K-
266 feldspar, biotite and amphibole phenocryst (less than 3mm in diameter) embedded in a fine-
267 grained silicic matrix (Fig. 5c). The zircon population contains grains (30-140 μm in diameter)
268 from subrounded subhedral to prismatic euhedral. Prisms are equant to moderately elongate
269 showing simple internal structure characterized by concentric and sector zoning to unzoned. A
270 concentric zoned or unzoned rim surrounds unzoned cores of few composite grains. A total of
271 37 U-Th-Pb SHRIMP analyses for sample SCV-30 yielded U content ranging from 74 to 4290
272 ppm. 25 analyses were obtained for zircon with discordance $\leq 5\%$, distributed along the
273 concordia curve from ca. 355 to 288 Ma, and yielded a weighted mean $^{208}\text{Pb}/^{238}\text{Th}$ age of $315 \pm$
274 6 Ma (mean square of weighted deviates, MSWD = 12; Fig. 7a). Some of the spread observed
275 could be due to the presence of inheritance. The oldest 10 grains yielding $^{206}\text{Pb}/^{238}\text{U}$ ages of c.
276 355-337 Ma probably represent xenocrysts derived from the Toca da Moura volcano-
277 sedimentary complex. Eleven grains in the age range ca. 334-311 Ma yielded a weighted mean
278 $^{208}\text{Pb}/^{238}\text{U}$ age of 318 ± 2 Ma (MSWD = 0.95; Fig. 7a), which is regarded as the best estimate
279 for the crystallization age of subvolcanic silicic rock.

280

281 **4.3. Cobble of granite found in a conglomerate from the Santa Susana Formation**

282 Sample SCV-7 is a cobble (20 cm in diameter) of pinkish medium-grained granite consisting of
283 quartz, alkali feldspar and biotite (Fig. 5d). Most zircons are stubby and elongated subeuhedral
284 to euhedral prisms (80 to 150 μm in diameter). Morphologically zircon grains are mostly simple
285 showing concentric zoning, sector zoning to unzoned, and few are composite with irregular and
286 unzoned small cores surrounded by a rim with concentric zoning. 40 U-Th-Pb SHRIMP
287 analyses were performed on sample SCV-7 with U content ranging from 348 to 3177 ppm. Of
288 this total of analyses 24 U-Pb ages with discordance $\leq 5\%$, scattered along the concordia curve
289 from ca. 349 to 294 Ma, yielded a weighted mean $^{206}\text{Pb}/^{238}\text{U}$ age of 327 ± 7 Ma (MSWD = 4;
290 Fig. 7b). A group of six zircon grains in the age range of c. 309-294 Ma yielded a weighted
291 mean $^{206}\text{Pb}/^{238}\text{U}$ age of 303 ± 6 Ma (MSWD = 0.98; Fig. 7b), which is taken as the probable
292 crystallization age of the granite. The remaining 19 zircon grains yielded $^{206}\text{Pb}/^{238}\text{U}$ ages of c.
293 349-326 Ma, suggesting inheritance.

294

295 **4.4. Siliciclastic rocks from the Toca da Moura and Cabrela volcano-sedimentary**
296 **complexes**

297 Sample TM-3 is a laminated poorly-sorted siltstone with quartz-rich silt layers, containing
298 feldspar and tourmaline grains, and lithoclasts (Fig. 5e), which are intercalated with darker
299 layers of clay. The zircon population is mostly characterized by stubby to elongated prismatic
300 small grains (less than 100 μm in diameter). It includes simple and composite zircons showing
301 concentric, sector and banded zoning. Of a total of 82 U-Th-Pb LA-ICP-MS analyses, with U
302 content ranging from 19 to 4630 ppm. 36 zircon grains yield 90-110% concordance. The
303 number grains of sample TM-1 is not conform to the minimum of 60-100 grains often used in
304 provenance studies (Vermeesch, 2004), and therefore percentages based on the proportions of
305 ages need to be interpreted with caution. The Paleozoic population of detrital zircon (36%)
306 includes Early Carboniferous (9%, c. 353, 349 and 340 Ma), Ordovician (14%, c. 476-456 Ma),
307 Cambrian (7%, c. 531-500 Ma) and Late Devonian (6%, c. 369 and 362 Ma) grains (Fig. 8a).
308 The Precambrian population (64%) is predominantly Neoproterozoic (36%; c. 983-587 Ma), but
309 also includes Paleoproterozoic (14%; c. 2-1.8 Ga), Mesoproterozoic (8%; c. 1.3-1 Ga) and
310 Archean (6%; c. 2.7-2.5 Ga) grains. The three youngest zircon grains (c. 353-340 Ma) yielded a
311 maximum depositional age of c. 348 Ma (Tournaisian), which is in accordance with the
312 sedimentary age inferred from biostratigraphic constraints (Late Tournaisian to Middle-Late
313 Viséan; Pereira et al., 2006; Lopes et al., 2014).

314 Sample CBR-11 is a fine-grained poorly-to-moderate sorted siltstone consisting predominantly
315 of quartz and few feldspar grains and lithoclasts enclosed in silt-clay-sized particles (Fig. 5g).
316 Most of zircon grains are small (less than 100 μm in diameter), euhedral to subeuhedral. They
317 are simple grains (short, stubby to equant prisms) with oscillatory concentric and banded
318 zoning, and only few are composite grains with rounded cores. Of a total of 20 U-Th-Pb LA-
319 ICP-MS analyses, with U content ranging from 54 to 1379 ppm, 10 grains yielded 90-110% of
320 concordance. Five grains are Paleozoic (Carboniferous: c. 359, 351 and 346 Ma; Cambrian: c.
321 514 and 511 Ma) and five are Precambrian (Paleoproterozoic: c. 2.4, 2.1 and 1.8 Ga;
322 Mesoproterozoic: 1 Ga; Neoproterozoic: c. 603 Ma). By combining our new data with those
323 from sample OM-200 (Pereira et al., 2012a) collected from the same quarry of sample CBR-11,
324 it was found that the detrital zircon population (CB, N = 54; Fig. 8a) is largely dominated by
325 Paleozoic grains (90%): Late-Middle Devonian (68%), Early Carboniferous (15%), Cambrian
326 (4%) and Early Devonian (2%) grains, being distinct from sample TM-3 described above (Fig.
327 8a). The number grains of sample CB (N=54), despite being larger than that of sample TM-1, is
328 not conform to the minimum of 60-100 grains, and therefore the proportions of ages obtained
329 also need to be interpreted with caution. The youngest zircon population (N = 5) ranging from c.
330 353 to 346 Ma), suggest a Tournaisian maximum depositional age which is slightly older than

331 the sedimentary age inferred from biostratigraphic constraints (Late Tournaisian to Middle-Late
332 Viséan; Pereira et al., 2006).

333

334 **4.5. Siliciclastic rocks from the Santa Susana Formation**

335 Sample SS-2 represents medium-to-coarse grained poorly-sorted sandstone. It is mainly
336 composed of lithoclasts (siltstone, mudstone, quartzite, phyllite, rhyolite, basalt) and quartz
337 grains, but also includes muscovite and feldspar grains (Fig. 5g). The zircon population is
338 mostly characterized by stubby to prismatic, subrounded to subangular, grains (120-300 μm in
339 diameter). Morphologically were found simple and composite grains. Cathodoluminescence
340 imaging shows that most zircon grains have concentric oscillatory zoning, irregular zoning and
341 are banded or unzoned. A total of 153 U-Th-Pb LA-ICP-MS analyses were performed on
342 detrital zircon grains. They show U content ranging from 15 to 6158 ppm. A population with 51
343 grains yielding U-Pb ages with 90-110% concordance (Fig. 8b) is dominated by Precambrian
344 ages (64%): Neoproterozoic (37%; c. 801-551 Ma), Paleoproterozoic (25%; c. 2.4-1.6 Ga) and
345 Neorchean (2%, c. 2.5 Ga). The Paleozoic grains (36%) are Carboniferous (20%; c. 359-303
346 Ma), Late Devonian (14%; c. 378-362 Ma), and Early Ordovician (2%; c. 447 Ma). The
347 youngest two grains (303 \pm 4 Ma; Kasimovian-Gzhelian) are slightly younger than the
348 sedimentary age inferred from biostratigraphic constraints (Middle Moscovian to Kasimovian;
349 Lemos de Sousa and Wagner, 1983; Machado et al., 2012; Lopes et al., 2014).

350 Sample SS-1 represents a very-coarse grained sandstone consisting of rounded-to-subangular
351 mono- and polycrystalline quartz, feldspar and muscovite grains, and a wide variety of
352 lithoclasts (chert, phyllite, rhyolite, siltstone and sandstone; Fig. 5h) . Zircon grains are rounded
353 to subangular, stubby and elongated prisms (less than 280 μm in diameter). The zircon
354 population includes simple grains with oscillatory concentric, banded and sector zoning, and
355 composite grains with cores with distinct internal morphologies surrounded by variable width
356 rims. A total of 150 U-Th-Pb LA-ICP-MS analyses performed on detrital zircon grains yielded
357 U content ranging from 24 to 9819 ppm. A group of 71 grains yielding U-Pb ages with 90-
358 110% concordance are dominated by Paleozoic ages (82%), predominantly made up of
359 Carboniferous (49%; c. 358-315 Ma) and Devonian (25%; c. 389-359 Ma), and a few Late
360 Ordovician-Silurian (5%; c. 434, 429 and 425 Ma) and Cambrian (3%; c. 533 and 491 Ma)
361 grains (Fig. 8b). The Precambrian grains (18%) are Neoproterozoic (10%; c. 702-542 Ma),
362 Paleoproterozoic (4%; c. 2.1-1.6 Ga), Mesoproterozoic (3%, c. 1.4 and 1.6 Ga) and Neorchean
363 (1%, c. 2.8 Ga). The youngest zircon population (N = 3; c. 319-315 Ma) suggest a Bashkirian
364 maximum depositional age, which is slightly older than the sedimentary age inferred from
365 biostratigraphic constraints (Middle Moscovian to Kasimovian; Lemos de Sousa and Wagner,
366 1983; Machado et al., 2012; Lopes et al., 2014).

367

368 **5. K-S test and MDS analysis: results**

369 We recognize that the representativeness of the detrital zircon grains of samples TM-1 and CB
370 is not the most recommended for provenance analysis. However, we consider important to
371 present a preliminary comparison of detrital zircon populations of Viséan marine siliciclastic
372 rocks from the Toca da Moura and Cabrela volcano-sedimentary complexes because it makes us
373 suspect of variability in the sources. A table showing the K-S results (referred to as Fig. S1
374 throughout the text) can be found in the supplementary data repository (available online at ...).
375 The K-S test performed on the Santa Susana sandstones show that the detrital zircon
376 populations of sample SS-2 (lower member) and SS upper member (i.e. includes samples StSz2
377 and StSz4 from Dinis et al., 2018) are ‘not significantly different’ (all ages- P-value = 0.169;
378 pre-Carboniferous ages- P-value = 0.879) at the 5% confidence level (Fig. S1). A comparison of
379 samples SS-1 and SS-2 reveals that they are “significantly different” (P-value \leq 0.01). Unlike
380 sample SS-2, the sample SS-1 detrital zircon population is “significantly different” (P-value <
381 0.01) from the SS upper population (Fig. S1), indicating that they derived from distinct sources.
382 Besides this, sample SS-1 is much closer to that of the SS upper (D-value = 0.323), and more
383 distant from sample SS-2 (D-value = 0.465) as regards the distance between cumulative
384 probability curves (Fig. 8c).

385 In Figure 9a, the MDS diagram produced with all ages shows sample SS-1 adjacent to Cabrela
386 and Mértola siliciclastic rocks, while sample SS-2 is near the Mira, Santa Iria and Represa
387 detrital zircon populations. In the MDS diagram for pre-Carboniferous ages, sample SS-2 is
388 juxtaposed with sample TM-3, and closest to the Mira, Phyllite-Quartzite and Tercenas
389 formations (Fig. 9b) suggesting likely sources. Nevertheless, the probable contribution to SS-2
390 samples of sediment derived from the oldest siliciclastic rocks from the PLZ and SPZ (i.e. Pulo
391 do Lobo, Gafo, Ribeira de Limas, Atalaia and Ronquillo formations), and OMZ sources cannot
392 be excluded. Their detrital zircon populations are ‘not enough significantly different’ (all ages-
393 P-value = 0.003), and ‘not significantly different’ (pre-Carboniferous ages- P-value = 0.113-
394 0.165) at the 5% confidence level (Fig. S1). This similarity is also illustrated in the
395 approximation between SS-2, P-G-R-A-R and OMZ populations in the MDS diagrams (Figs.
396 9a, b).

397 K-S test results for the comparison between samples SS-2 and TM-3 indicate that they present
398 ‘not significantly different’ detrital zircon populations (all ages- P-value = 0.399; pre-
399 Carboniferous ages- P-value = 0.0411) at the 5% confidence level (Fig. S1). Furthermore, their
400 cumulative probability curves are much closer (Fig. 8d): D-values are 0.195 (all ages) and 0.203
401 (pre-Carboniferous ages) (Fig. S1). The close relationship of the two detrital zircon populations
402 suggests that the Toca da Moura volcano-sedimentary complex directly supplied sediment to the
403 Santa Susana basin. However, the relationship described above does not extend to the entire
404 Santa Susana basin since sample SS-1 presents a greater degree of similarity with the Cabrela

405 detrital zircon population as regards the proximity between cumulative probability curves (Fig.
406 8d) and MDS diagrams (Figs. 9a, b).

407 In addition, Cabrelas siliciclastic rocks are ‘significantly different’ at the 5% confidence level
408 from sample TM-3 (P-values < 0.01) as regards the significant distance between them on the
409 MDS diagram (Figs. 9a, b), and the significant distance between cumulative curves (Fig. 8d),
410 with a D-value interval of 0.712-0.731 (Fig. S1). The difference found in the detrital zircon
411 populations suggests that Cabrelas and Toca da Moura siliciclastic rocks probably derived from
412 different sources.

413 As result of the K-S test and MDS analysis, the Horta da Torre Formation is ‘significantly
414 different’ (Fig. S1), and is clearly separate (Figs. 9a, b) from all the other detrital zircon
415 populations, ruling out the possibility of it being a source for the Toca da Moura and Cabrelas
416 volcano-sedimentary complexes or Santa Susana Formation siliciclastic rocks.

417

418 **6. Discussion**

419 **6.1. Chronostratigraphic framework**

420 The geochronological data presented in the present study provide the basis for the first
421 chronostratigraphic record for the Carboniferous basins of the Santa Susana-São Cristovão
422 region (SW Iberia). Dating of silicic volcanic rocks interbedded in the Toca da Moura and
423 Cabrelas volcano-sedimentary complexes constrain an interval of felsic magmatism to occurring
424 from c. 335 Ma to 331 Ma (Viséan; Fig. 6), complementing currently-available biostratigraphic
425 information for Toca da Moura and Cabrelas siliciclastic rocks (Pereira et al., 2006; Lopes et al.,
426 2014). U-Pb ages of the youngest detrital zircon grains from the siliciclastic rocks of the Toca
427 da Moura and Cabrelas volcano-sedimentary complexes (TM-3 and CB, respectively; Fig. 8a)
428 provide maximum age constraints for these marine deposits. Their maximum depositional ages
429 (c. 351-348 Ma; Tournaisian) are slightly older than currently-available biostratigraphic ages
430 (Pereira et al., 2006; Lopes et al., 2014), but provide confirmation that both marine deposits are
431 broadly contemporaneous.

432 Furthermore, the best estimate of the crystallization age of the Baleizão silicic intrusion
433 provides a minimum age of 318 ± 2 Ma (Bashkirian; Fig. 7a) for the intra-Carboniferous
434 unconformity. Zircon extracted from a pebble of granite found in a Santa Susana conglomerate
435 yielded a crystallization age of c. 303 Ma for plutonic rock (Fig. 7b). This age estimate overlaps
436 the age interval of c. 305-303 Ma (i.e. the maximum depositional age range) obtained for the
437 youngest population of detrital zircon grains from sandstone of the upper member (Dinis et al.,
438 2018), complementing the currently-available biostratigraphic information for the Santa Susana
439 Formation (Machado et al., 2012; Lopes et al., 2014). Given the findings described above, a
440 stratigraphic interval of approximately 13-17 Ma can be established for the intra-Carboniferous
441 unconformity, marking a change in depositional environment from marine to terrestrial in the

442 OMZ. Basin-drainage and infill patterns most probably changed due to rapid uplift of the
443 Variscan-Appalachian orogenic belt, active during the waning stages of Laurussia-Gondwana
444 collision (i.e. Late Carboniferous).

445

446 **6.2. Provenance and evolutionary model**

447 An initial important finding provides evidence that they derived from different sources. The
448 TM-3 population presents 64% Precambrian detrital zircon grains, while the CB population
449 contains only 10% (Fig. 8a). Toca da Moura siliciclastic rocks have a greater affinity with the
450 Phyllite-Quartzite, Tercenas, Santa Iria and Represa formations (Fig. 9), indicating that detrital
451 zircon populations were reproduced faithfully in SPZ and PLZ (Laurussian-type) sources. A
452 contribution from the oldest siliciclastic sequences of PLZ (Pulo do Lobo, Atalaia, Gafo and
453 Ribeira de Limas formations) and OMZ (Gondwanan-type) sources cannot be ruled out for
454 sample TM-3 (Fig. 9). The number of Late-Middle Devonian zircon grains in sample TM-3
455 (6%) is smaller than that of the CB population (68%) (Fig. 8a), suggesting that Cabrela
456 siliciclastic rocks were most likely derived largely from a Devonian source consistent with a
457 limited contribution from recycled ancient rocks (Pereira et al., 2012a). This indicates that the
458 origin of the Visean Toca da Moura and Cabrela basins is most likely more closely linked to
459 sources located in the SPZ and PLZ (Laurussian-type) than in the OMZ (Gondwanan-type). The
460 evidence in the Visean Toca da Moura basin for dissection of the inactive Devonian magmatic
461 arc and the erosion of its plutonic roots, together with the recycling of the PLZ and SPZ
462 Frasnian-Tournaisian siliciclastic sequences and OMZ basement rocks, differs from the
463 evidence in the Cabrela basin. The significance of the involvement of distinct sources is that
464 part of the region located on the boundary between the OMZ- PLZ and the SPZ (SW Iberia) was
465 subjected to uplift while the remaining part underwent flexural subsidence. A similar tectonic
466 setting has been put forward as an explanation for differences in stratigraphy found in the
467 Pedroches syn-orogenic basin located along the OMZ-Central Iberian Zone boundary
468 (Armendáriz et al., 2008, and references therein) (Fig. 1).

469 Over the past four decades, different models have emerged to explain the geodynamic evolution
470 of SW Iberia, with the subduction polarity being widely discussed (Quesada et al., 1994; Castro
471 et al., 1996; Ribeiro et al., 2007; Pin et al., 2008; Simancas et al., 2009; Braid et al., 2011;
472 Pérez-Cáceres et al. 2015a; Díez Fernández et al., 2016; Pereira et al., 2017a). Although in
473 many paleogeographic reconstructions for the Devonian, Iberia is flanked by the Rheic and
474 Paleotethys oceans (Stampfli et al., 2002, 2013; Cocks and Torsvik, 2006; Stampfli and Kozur,
475 2006; Torsvik et al., 2012; Arenas et al., 2014; von Raumer et al., 2016), solely the subduction
476 of Rheic Ocean is considered in the present geodynamic models for Iberia. This geodynamic
477 model of a single ocean has been the trigger of numerous discussions about whether the active
478 magmatic arc was located in Laurussia or Gondwana margins. Our challenging recent proposal

479 considers that SW Iberia geodynamic evolution could have been linked to the closure of these
480 two oceanic basins (Pereira et al., 2020). The main assumption that we must assume is that SPZ
481 and PLZ (Laurussian-side) and OMZ (Gondwana-side) have experienced different and
482 independent geodynamic evolutions before they were juxtaposed by the Variscan sinistral
483 orogen-parallel motion (Pérez-Cáceres et al., 2015b). As illustrated in Figure 10a, the
484 subduction of the Rheic Ocean floor beneath the Laurussian margin during the Late Devonian
485 (Pérez-Cáceres et al., 2015a; Pereira et al., 2017a, and references therein) caused the onset of
486 the Rheic magmatic arc in the Meguma terrane and related synorogenic basins. A slab rollback
487 mechanism similar to the one that caused the opening of the Okinawa trough behind the
488 Ryukyu-type subduction in the Pacific Ocean (Yamaji, 2003; Boutelier and Cruden, 2013)
489 could explain the lithosphere extension in the Laurussian-side and the Late Devonian
490 siliciclastic sedimentation in SPZ and PLZ (Pereira et al., 2017a). The Laurussian active margin
491 was progressively accreted to the Gondwana passive margin facing the Rheic Ocean during the
492 Late Devonian (Fig. 10a). A nappe stack was gradually emplaced in the Gondwana margin as a
493 consequence of ongoing continental collision (Pérez-Cáceres et al., 2015a; Díez Fernández and
494 Arenas, 2015, and references therein; Díez Fernández et al., 2016) and orogenic gravitational
495 collapse (Dias da Silva et al., 2020). Following the closure of the Rheic, Tournaisian, magmatic
496 episodes were associated with lithospheric extension in the Laurussian (Pyrite belt volcano-
497 sedimentary complex and Gil Márquez pluton) and Gondwanan (Beja igneous complex)
498 margins. A mechanism of steepening and break-off of the Rheic Ocean slab beneath the
499 Laurussian margin, as the modern analog of Eastern Anatolia Alpine-Himalaya collisional
500 mountain belt (Sengor et al., 2003; Keskin, 2007), possibly was the main the reason for the
501 Early carboniferous magma generation in the SPZ (Pin et al. 2008), simultaneously the Meguma
502 terrane experienced rapid uplift and terrestrial sedimentation (Fig. 10b1). At the same time, in
503 the Gondwanan-side, the upwelling of the asthenosphere could have triggered partial melting of
504 crustal materials, and lithosphere extension (Pereira et al., 2009; 2012b), creating the right
505 conditions for the onset of gneiss domes in the OMZ (Dias da Silva et al., 2018). The
506 emplacement of voluminous subduction-related magmas (Santos et al., 1990; Castro et al.,
507 1996; Jesus et al., 2007; Pin et al., 2008; Lima et al., 2012; Pereira et al., 2007, 2015a; Moita et
508 al., 2009, 2015), including some with boninitic (Castro et al., 1999) and adakitic (Lima et al.,
509 2013) affinities, was coeval with flexural subsidence, marine sedimentation and volcanism
510 (Toca da Moura, Cabrela, Los Pedroches basins) (Fig. 10b2). The Early Carboniferous thermal
511 anomaly recorded in the OMZ has been interpreted to result from the emplacement in the
512 middle crust of a large volume of mantle plume-related magmas (Simancas et al., 2006). Other
513 studies have suggested that voluminous Early Carboniferous magmatism could have resulted
514 from the subduction of an oceanic ridge, creating a slab window beneath the OMZ (Castro et al.,
515 1996, 1999; Diaz-Azpiroz et al., 2006). This model uses the Chile ridge that plunges beneath

516 South America Plate in Patagonia (Breitsprecher and Thorkelson, 2009) as modern analog. Our
517 model assumes the subduction of a ridge of the Paleotethys Ocean lithosphere beneath the
518 Gondwana margin (Fig. 10b2), instead of the Rheic Ocean lithosphere, as a hypothesis to be
519 further explored since the magmatic activity has extended to the Serpukhovian and Bashkirian
520 in the OMZ (Pavia pluton, Valencia del Ventoso plutonic complex and Baleizão porphyry).
521 Simultaneously with the putative subduction of the Paleotethys Ocean ridge, other regions of
522 the Appalachian-Variscan orogenic belt, mostly in the Laurussian-side (Fig. 10b1), have
523 experienced an oblique collision, rapid uplift and terrestrial sedimentation (Pereira et al., 2020).
524 A second significant finding is that detrital zircon populations from the Santa Susana Formation
525 (samples SS-1 and SS-2) also show significant differences (Figs. 8 and 9). Basal conglomerate
526 (sample SS-2) presents a greater percentage of Precambrian grains (64%) than uppermost
527 sandstone (SS-1 sample; 28%), and presents a great degree of affinity with the detrital zircon
528 population of sample TM-3. Sample SS-2 presents a great degree of similarity with the detrital
529 zircon populations of overlying SS upper-member sandstones (samples StSz-2 and StSz-4;
530 Dinis et al., 2018) sampled as part of the same stratigraphic profile. SS-2 and SS upper-age
531 populations show a great degree of affinity (Fig. 9), suggesting that detrital zircon grains were
532 mainly derived from the erosion of the Toca da Moura volcano-sedimentary complex, the Santa
533 Iria and Represa formations (PLZ) and the Mira Formation (SPZ). However, regarding the
534 detrital zircon grains with pre-Carboniferous ages, additional contributions from other PLZ
535 (Pulo do Lobo, Atalaia, Gafo and Ribeira de Limas formations), SPZ (Brejeira, Phyllite-
536 Quartzite, Tercenas and Ronquillo formations) and OMZ sources cannot be ruled out (Figs. 9a,
537 c). The zircon age population of sample SS-1, which is distinct from the SS-2 population,
538 presents a great degree of affinity with the CB population, suggesting lateral changes in sources
539 during deposition of Santa Susana uppermost sandstones. The great degree of affinity of the SS-
540 1, Cabrela volcano-sedimentary complex, with Mértola Formation detrital zircon populations
541 suggests a close association between the two and a common source. Cabrela and Mértola
542 siliciclastic rocks may be regarded as the main source for sample SS-1 and an intermediate
543 sediment repository as they are derived from the erosion of a Devonian source partially
544 represented by the Cercal porphyries from the SPZ. As result of rapid uplift, the progressive
545 erosion of the Devonian magmatic arc (including its plutonic roots), and that of PLZ, SPZ and
546 OMZ rocks, is evidenced in the Santa Susana Formation. The volumetrically significant
547 contribution of Carboniferous sources to the Santa Susana basin fill confirms derivation from
548 the erosion of: i) Pyrite Belt volcanic rocks, and Phyllite-Quartzite, Tercenas, Mértola, Mira and
549 Brejeira siliciclastic rocks (SPZ); ii) the Santa Iria and Represas formations (PLZ); iii) Gil
550 Marquez granitic rocks and other plutons of the Sierra del Norte Batholith (SPZ and PLZ); iv)
551 the Beja igneous complex, which includes the Baleizão porphyries (OMZ), and Évora and Pavia
552 plutonic and high-grade metamorphic rocks (OMZ); and v) the Cabrela and Toca da Moura

553 volcanic-sedimentary complexes (OMZ) and Mértola turbidites (SPZ). From Late
554 Carboniferous to Early Permian, large-scale strike-slip motions have juxtaposed OMZ to PLZ
555 and SPZ (García-Navarro and Fernández, 2004; Pérez-Cáceres et al., 2015b), simultaneously
556 with the rapid uplift of Variscan orogenic belt (Fig. 10c). In Kasimovian-Ghzelian,
557 sedimentation probably occurred through the opening of the pull-apart terrestrial basin (Santa
558 Susana basin) related to the movement of major strike-slip faults (i.e. Porto-Tomar fault zone,
559 Pereira et al., 2010; Machado et al., 2012; Gutiérrez-Alonso et al., 2015) during the progressive
560 uplift and buckling of the linear Appalachian-Variscan orogenic belt (i.e. OMZ, PLZ and SPZ;
561 Fig. 10c), related to a change in the regional stress-field that produced the Greater Cantabrian
562 Orocline (Pastor-Galan et al., 2015). U-Pb dating of magmatic zircon extracted from a pebble of
563 granite (c. 303 Ma; Fig. 7b) found in a conglomerate of the Santa Susana Formation lower
564 member suggests provenance from the direct erosion of Permo-Carboniferous plutons (i.e.
565 original primary source), such as Santa Eulália-Monforte granitic and gabbro-dioritic rocks
566 (OMZ). This c. 303-297 Ma calc-alkaline plutonic suite is coeval with the Nisa-Albuquerque
567 and Los Pedroches batholiths, located on the OMZ-Central Iberian Zone boundary (Fig. 1),
568 probably representing magmatism related to the eastward-migration of the Paleotethyan arc
569 (Permo-Carboniferous Pyrennes plutonic and volcanic rocks; Pereira et al., 2014; Pereira et al.,
570 2015b, 2017b). The Permo-Carboniferous OMZ plutons were emplaced at shallow crustal levels
571 consistent with the low assimilation of country rocks and the sharp contacts, and therefore, they
572 may have experienced denudation shortly after its crystallization without being required
573 unrealistic uplift rates.

574

575 **7. Conclusions**

576 The main conclusions of this study are the following:

- 577 1. Viséan marine deposition in the Santa Susana-São Cristovão and Cabrela regions is
578 constrained to the age interval of c. 335-331 Ma by the new U-Pb data for volcanic rocks
579 intercalated within siliciclastic rocks of the Toca da Moura and Cabrela volcano-sedimentary
580 complexes.
- 581 2. U-Pb dating of the Baleizão porphyry provides a minimum age of 318 ± 2 Ma (Bashkirian) for
582 the overlying intra-Carboniferous unconformity.
- 583 3. Viséan siliciclastic rocks from the Cabrela and Toca de Moura volcano-sedimentary
584 complexes are derived from distinct sources, which probably include a Devonian continental
585 magmatic arc, and are likely to be more closely associated with the Laurussian-type sources
586 (SPZ and PLZ) than the Gondwanan-type sources (OMZ).
- 587 4. Terrestrial siliciclastic rocks from the Santa Susana Formation are probably the result of the
588 recycling of distinct sources associated with the SPZ, PLZ and OMZ.

589 5. The best estimate of crystallization of a granite pebble found in Santa Susana Formation
590 conglomerate suggest a maximum depositional age of c. 303 Ma (Kasimovian-Gzhelian);
591 together with the youngest U-Pb ages (< c. 318 Ma) of detrital zircon grains, these findings
592 provide evidence of the denudation of primary crystalline sources during the rapid post-
593 accretion/collision uplift of the Variscan orogenic belt in SW Iberia (i.e. Gondwanan- and
594 Laurussian-type sources).
595 6. The intra-Carboniferous unconformity that separates the Toca da Moura volcano-complex
596 and the Baleizão porphyry from the Santa Susana Formation indicates a notable time interval of
597 approximately 13-17 Ma.

598

599 **Acknowledgements**

600 This work is a contribution to projects CGL2016-76438-P and PGC2018-096534-B-I00 (Spain),
601 the ICT's Research Group 6- Lithosphere Dynamics (ICT-UID/GEO/04683/2019) and, IDL's
602 Research Group 3- Solid Earth dynamics, hazards, and resources (Portuguese FCT). Í. Dias da
603 Silva acknowledges financial support by SYNTHESIS3-ACCESS (DE-TAF-5798), FCT
604 postdoctoral grant SFRH/BPD/99550/2014 and FCT-project UID/GEO/50019/2019-IDL. This
605 is IBERSIMS publication number 71.

606

607 **References**

608 Andrade, A.S.: Contribution à l'Analyse de la Suture Hercynienne de Beja (Portugal), Perspectives
609 Métallogéniques. Unpublished PhD thesis INPL, 137 p, 1983.
610
611 Andrade, C.F.: Alguns elementos para o estudo dos depósitos de carvão do Moinho da Ordem.
612 Comunicações dos Serviços Geológicos de Portugal, tomo XVI, 3-28, 1927.
613
614 Arenas, R., Díez Fernández, R., Sánchez Martínez, S., Gerdes, A., Fernández-Suárez, J. and Albert, R.:
615 Two-stage collision: exploring the birth of Pangea in the Variscan terranes. *Gondwana Research* 25, 756-
616 763, 2014.
617
618 Armendáriz, M., López-Guijarro, R., Quesada, C., Pin, C. and Bellido, F.: Genesis and evolution of a
619 syn-orogenic basin in transpression: Insights from petrography, geochemistry and Sm-Nd systematics in
620 the Variscan Pedroches basin (Mississippian, SW Iberia). *Tectonophysics* 461: 395-413, 2008.
621
622 Azor, A., Rubatto, D., Simancas, J.F., González Lodeiro, F., Martínez Poyatos, D., Martín Parra, L.M.
623 and Matas, J.: Rheic Ocean ophiolitic remnants in southern Iberia questioned by SHRIMP U-Pb zircon
624 ages on the Beja-Acebuches amphibolites. *Tectonics* 27, TC5006, doi:10.1029/2008TC002306, 2008.
625

626 Barbeau, D.L., Davis, J.T., Murray, K.E., Valencia, V., Gehrels, G.E., Zahid, K.M. and Gombosi, D.J.:
627 Detrital-zircon geochronology of the metasedimentary rocks of north-western Graham Land. *Antarctic*
628 *Science* 22, 65-78, 2009.

629

630 Boutelier, D. and Cruden, A.: Slab rollback rate and trench curvature controlled by arc deformation.
631 *Geology* v. 41; no. 8, 911-914, 2013.

632

633 Bowring, S.A., Schoene, B., Crowley, J.L., Ramezani, J. and Condon, D.J.: High-precision U-Pb zircon
634 geochronology and the stratigraphic record: Progress and promise. In: Olszewski, T. (Ed.),
635 *Geochronology: Emerging Opportunities*, Paleontological Society Short Course, October 21,
636 Philadelphia, PA., Paleontological Society Papers, Volume 11, 23-43, 2006.

637

638 Braid, J.A., Murphy, J.B., Quesada, C. and Mortensen, J.: Tectonic escape of a crustal fragment during
639 the closure of the Rheic Ocean: U–Pb detrital zircon data from the late Palaeozoic Pulo de Lobo and
640 South Portuguese Zones, Southern Iberia, *Journal of the Geological Society of London* 168, 383–392,
641 2011.

642

643 Breitsprecher, K. and Thorkelson, D.J.: Neogene kinematic history of Nazca-Antarctic-Phoenix slab
644 windows beneath Patagonia and the Antarctic Peninsula. *Tectonophysics* 464, 10-20, 2009.

645

646 Caldeira, R., Ribeiro, M.L. and Moreira, M.E. Geoquímica das sequências máficas e félsicas entre Alvito,
647 Torrão e Alcáçovas (SW da ZOM). *Comunicações Geológicas*, 94, 5-28, 2007.

648

649 Cambeses, A., Scarrow, J.H., Montero, P., Molina, J.F. and Moreno, J.A. SHRIMP U-Pb zircon dating of
650 the Valencia del Ventoso plutonic complex, Ossa-Morena Zone, SW Iberia: Early Carboniferous intra-
651 orogenic extension-related ‘calc-alkaline’ magmatism. *Gondwana Research* 28, 735-756, 2015.

652

653 Castro, A., Fernández, C., de la Rosa, J.D., Moreno-Ventas, I., El Hmidi, H., El Biad, M., Bergamin,
654 J.F. and Sánchez, N.: Triple-junction migration during Paleozoic Plate convergence: The Aracena
655 metamorphic belt, Hercynian massif, Spain, *Geologische Rundschau.*, 85, 108-185, 1996.

656

657 Castro, A., Fernández, C. El-Hmidi, H., El-Bia, M. Díaz Azpiroz, M., de la Rosa, J.D. and Stuart, F.: Age
658 constraints to the relationships between magmatism, metamorphism and tectonism in the Aracena
659 metamorphic belt, southern Spain, *International Journal of Earth Sciences*, 88, 26-37, 1999.

660

661 Chichorro, M., Pereira, M. F., Díaz-Azpiroz, M., Williams, I.S., Fernández, C., Pin, Ch., and Silva, J.B.:
662 Cambrian ensialic rift-related magmatism in the Ossa-Morena Zone (Évora-Aracena metamorphic belt,
663 SW Iberian Massif): Sm-Nd isotopes and SHRIMP zircon U-Th-Pb geochronology. *Tectonophysics*,
664 461, 91-113, 2008.

665

666 Cocks, L.R.M. and Torsvik, T.H.: European geography in a global context from the Vendian to the end of
667 the Palaeozoic. In: Gee, D.G., Stephenson, R.A. (eds). *European Lithosphere Dynamics*. Geological
668 Society, London, Memoirs, 32, 83-95, 2006.

669

670 DeGraaff-Surpless, K., Mahoney, J.B., Wooden, J.L. and McWilliams, M.O.: Lithofacies control in
671 detrital zircon provenance studies: insights from the Cretaceous Methow Basin, Southern Canadian
672 Cordillera. *Geological Society of America Bulletin*, 115(8), 899-915, 2003.

673

674 Dias da Silva, Í., González Clavijo, E. and Díez-Montes, A.: The collapse of the Variscan belt: a Variscan
675 lateral extrusion thin-skinned structure in NW Iberia. *International Geology Review*,
676 <https://doi.org/10.1080/00206814.2020.1719544>, 2020.

677

678 Dias da Silva, Í., Pereira, M.F., Silva, J.B., and Gama, C.: Time-space distribution of silicic plutonism in
679 a gneiss dome of the Iberian Variscan Belt: The Évora Massif (Ossa-Morena Zone, Portugal).
680 *Tectonophysics* 747-748, 298-317, 2018.

681

682 Díaz Azpiroz, M., Fernandez, C., Castro, A. and El-Biad, M.: Tectonometamorphic evolution of the
683 Aracena metamorphic belt (SW Spain) resulting from ridge-trench interaction during Variscan plate
684 convergence. *Tectonics* 25, <http://dx.doi.org/10.1029/2004TC001742>, 2006.

685

686 Dickinson, W.R. and Gehrels, G.E.: Use of U-Pb ages of detrital zircons to infer
687 maximum depositional ages of strata: a test against a Colorado Plateau Mesozoic database. *Earth and
688 Planetary Science Letter* 288, 115-125, 2009.

689

690 Díez Fernández, R., Arenas, R., Pereira, M.F., Sánchez Martínez, S., Albert, R., Martín Parra, L.M.,
691 Rubio Pascual, F.J. and Matas, J.: Tectonic evolution of Variscan Iberia: Gondwana-Laurussia collision
692 revisited. *Earth-Science Reviews* 162, 269–292, 2016

693

694 Díez Fernández, R. and Arenas, R.: The Late Devonian Variscan suture of the Iberian Massif: a
695 correlation of high-pressure belts in NW and SW Iberia. *Tectonophysics* 654, 96-100, 2015.

696

697 Dinis, P.A., Fernandes, P., Jorge, R.C.G.S., Rodrigues, B., Chew, D.M. and Tassinari, C.G.: The
698 transition from Pangea amalgamation to fragmentation: constraints from detrital zircon geochronology on
699 West Iberia paleogeography and sediment sources. *Sedimentary Geology* 375, 172-187, 2018.

700

701 Domingos, L.C.G., Freire, J.L.S., Silva, F. G., Gonçalves, F., Pereira, E. and Ribeiro, A.: The Structure of
702 the Intramontane Upper Carboniferous Basins in Portugal. In: M. J. Lemos de Sousa, J.T. Oliveira (eds.),
703 *The Carboniferous of Portugal*. Memórias, Nova Série 29, Serviços Geológicos de Portugal, Lisboa: 187-
704 194, 1983.

705

706 Fedo, C.M., Sircombe, K.N. and Rainbird, R.H.: Detrital zircon analysis of the sedimentary record. In:
707 Zircon (eds. M. Hanchar & P.W.O. Hoskin) Reviews in Mineralogy and Geochemistry, 53, 277-303.
708 Mineral Society of America, Washington, DC, 2003.
709

710 Ferreira, P., Caldeira, R. and Calvo, R.: Geoquímica das rochas ígneas aflorantes na região de S. Matias,
711 Cuba (Alentejo). Comunicações Geológicas (2014) 101, Especial I, 93-97, 2014.
712

713 Fonseca, P., Munhá, J., Pedro, J., Rosas, F., Moita, P., Araújo, A. and Leal, N.: Variscan ophiolites and
714 high-pressure metamorphism in southern Iberia. *Ofioliti* 24, 259-268, 1999.
715

716 Frei, D. and Gerdes, A.: Precise and accurate in-situ U–Pb dating of zircon with high sample throughput
717 by automated LA-SF-ICP-MS. *Chemical Geology* 261(3-4): 261-27, 2009.
718

719 Gama, C., Pereira, M.F., Crowley, Q.G., Dias da Silva, Í. and Silva, J.B.: Detrital zircon provenance of
720 Triassic sandstone of the Algarve Basin (SW Iberia): Evidence of Gondwanan- and Laurussian-type
721 sources of sediment. *Geological Magazine*, <https://doi.org/10.1017/S0016756820000370>, 2020.
722

723 García-Navarro, E. and Fernández, C.: Final stages of the Variscan Orogeny at the southern Iberian
724 massif: Lateral extrusion and rotation of continental blocks. *Tectonics* 23, TC6001,
725 DOI:10.1029/2004TC001646, 2004.
726

727 Gehrels, G.E.: Detrital zircon U-Pb geochronology applied to tectonics. *Annual*
728 *Review of Earth and Planetary Sciences* 42: 127-149, 2014.
729

730 Gonçalves, F. and Carvalhosa, A.: Subsídios para o conhecimento geológico do Carbónico de Santa
731 Susana Vol. D' Hommage au géologue G. Zbyszewski. *Recherche de Civilisations*, Paris, pp. 109-130,
732 1984.
733

734 Gutiérrez-Alonso, G., Collins, A.S., Fernández-Suárez, J., Pastor-Galán, D., González-Clavijo, E.,
735 Jourdan, F., Weil, A.B., and Johnston, S.T.: Dating of lithospheric buckling: $^{40}\text{Ar}/^{39}\text{Ar}$ ages of syn-
736 orocline strike-slip shear zones in northwestern Iberia: *Tectonophysics*, 643, 44-54, 2015.
737

738 Gynn, J. and Gehrels, G.: Comparison of Detrital Zircon Age Distributions Using the K-S Test. Arizona
739 LaserChron Center. Available at: <https://laserchron.org/>, 2010
740

741 Jesus, A., Munhá, J., Mateus, A., Tassinari, C. and Nutman, A.: The Beja layered gabbroic sequence
742 (Ossa–Morena Zone, Southern Portugal): geochronology and geodynamic implications. *Geodinamica*
743 *Acta* 20, 139-157, 2007.
744

745 Jesus, A.P., Mateus, A., Munhá, J.M., Tassinari, C.G., Bento dos Santos, T.M. and Benoit, M.: Evidence
 746 for underplating in the genesis of the Variscan synorogenic Beja
 747 Layered Gabbroic Sequence (Portugal) and related mesocratic rocks. *Tectonophysics* 683: 148-171, 2016.
 748
 749 Keskin, M.: Eastern Anatolia: A hotspot in a collision zone without a mantle plume. In: Foulger, G.R.,
 750 Jurdy, D.M. (eds), *Plates, plumes, and planetary processes: Geological Society of America Special Paper*
 751 430, 693-722, 2007.
 752
 753 Lemos de Sousa, M.J. and Wagner, R.H.: General description of the terrestrial Carboniferous basins in
 754 Portugal and history of investigations. In: Lemos de Sousa M.J. and Oliveira, J.T., (eds) *The*
 755 *Carboniferous of Portugal. Memórias dos Serviços Geológicos de Portugal* 29:117-126, 1983.
 756
 757 Lima, S.M., Corfu, F., Neiva, A.M.R. and Ramos, M.F.: Dissecting complex magmatic processes: an in-
 758 depth U-Pb study of the Pavia Pluton, Ossa-Morena Zone, Portugal. *Journal of Petrology* 53, 1887-1911,
 759 2012.
 760
 761 Lima, S.M., Neiva, A.M.R. and Ramos, J.M.F.: Adakitic-like magmatism in western Ossa-Morena Zone
 762 (Portugal): Geochemical and isotopic constraints of the Pavia pluton. *Lithos* 160-161, 98-116, 2013.
 763
 764 Linnemann, U., Pereira, M.F., Jeffries, T., Drost, K. and Gerdes, A.: Cadomian orogeny and the opening
 765 of the Rheic Ocean: new insights in the diachrony of geo-tectonic processes constrained by LA-ICP-MS
 766 U-Pb zircon dating (Ossa-Morena and Saxo-Thuringian Zones, Iberian and Bohemian Massifs).
 767 *Tectonophysics* 461, 21-43, 2008.
 768
 769 Lopes, G., Pereira, Z., Fernandes, P., Wicander, R., Matos, J.X., Rosa, D. and Oliveira, J.T.: The
 770 significance of reworked palynomorphs (middle Cambrian to Tournaisian) in the Visean Toca da Moura
 771 Complex (South Portugal). Implications for the geodynamic evolution of Ossa Morena Zone. *Review of*
 772 *Palaeobotany and Palynology* 200, 1-23, 2014.
 773
 774 Ludwig, K.R.: *Isoplot/Ex Version 3.0: a Geochronological Toolkit for Microsoft Excel*, 2003.
 775
 776 Machado, G., Dias da Silva, I. and Almeida, P.: Palynology, stratigraphy and geometry of the
 777 Pennsylvanian continental Santa Susana Basin (SW Portugal). *Journal of Iberian Geology* 38, 429-448,
 778 2012.
 779
 780 Moita, P., Santos, J.F. and Pereira, M.F.: Layered granitoids: interaction between continental crust
 781 recycling processes and mantle-derived magmatism. Examples from the Évora Massif (Ossa-Morena
 782 Zone, southwest Iberia, Portugal). *Lithos* 111, (3-4): 125-141, 2009.
 783

784 Moita, P., Santos, J.F., Pereira, M.F., Costa, M.M. and Corfu, F.: The quartz-dioritic Hospitais intrusion
785 (SW Iberian Massif) and its mafic microgranular enclaves -evidence for mineral clustering. *Lithos* 224-
786 225, 78-100, 2015.

787

788 Oliveira, J.T., Oliveira, V. and Piçarra, J.: Traços gerais da evolução tectono-estratigráfica da Zona de
789 Ossa Morena, em Portugal. *Cuadernos do Laboratorio Xeoloxico de Laxe* 16, 221-250, 1991.

790

791 Pastor-Galán, D., Ursem, B., Meere, P.A., and Langereis, C.: Extending the Cantabrian Orocline to two
792 continents (from Gondwana to Laurussia). *Paleomagnetism from South Ireland. Earth and Planetary*
793 *Science Letters* 432, 223-231, 2015.

794

795 Pereira, M.F., Gama, C., Dias da Silva, Í., Fuenlabrada, J.M., Silva, J.B. and Medina, J.: Isotope
796 geochemistry evidence for Laurussian-type sources of South-Portuguese Zone Carboniferous turbidites
797 (Variscan orogeny). In: Murphy, J.B. (Eds). *Pannotia to Pangea: Neoproterozoic and Paleozoic orogenic*
798 *cycles in the circum-North Atlantic region. Geological Society of London, Special Publication, DOI:*
799 *10.1144/SP503-2019-163*, 2020.

800

801 Pereira, M.F., Martínez Poyatos, D., Pérez-Cáceres, I., Gama, C. and Azor, A.: Comment on
802 “Stratigraphy of the Northern Pulo do Lobo Domain, SW Iberia Variscides: A palynological
803 contribution” by Zélia Pereira et al. (2018) - *Geobios* 51, 491-506. *Geobios* 55: 103-106, 2019.

804

805 Pereira, M.F., Gutiérrez-Alonso, G., Murphy, J.B., Drost, K., Gama, C. and Silva, J.B.: Birth and demise
806 of the Rheic Ocean magmatic arc(s): Combined U-Pb and Hf isotope analyses in detrital zircon from SW
807 Iberia siliciclastic strata. *Lithos* 278-281, 383-399, 2017a.

808

809 Pereira, M.F., Gama, C. and Rodríguez, C.: Coeval interaction between magmas of contrasting
810 composition (Late Carboniferous-Early Permian Santa Eulália-Monforte massif, Ossa-Morena Zone):
811 field relationships and geochronological constraints. *Geologica Acta* 15, 409-428, 2017b.

812

813 Pereira, M.F., Chichorro, M., Moita, P., Santos, J.F., Solá, A.M.R., Williams, I.S., Silva, J.B. and
814 Armstrong, R.A.: The multistage crystallization of zircon in calc-alkaline granitoids: U-Pb age constraints
815 on the timing of Variscan tectonic activity in SW Iberia. *International Journal of Earth Sciences* 104, 5,
816 1167-1183, 2015a.

817

818 Pereira, M.F., Castro, A. and Fernández, C.: The inception of a Paleotethyan magmatic arc in Iberia.
819 *Geosciences Frontiers*: 6, 297-306, 2015b.

820

821 Pereira, M.F., Ribeiro, C., Vilallonga, F., Chichorro, M., Drost, K., Silva, J.B., Albardeiro, L., Hofmann,
822 M. and Linnemann, U.: Variability over time in the sources of South Portuguese Zone turbidites:

823 evidence of denudation of different crustal blocks during the assembly of Pangea. *International Journal of*
824 *Earth Sciences*, 103, 1453-1470, 2014a.

825

826 Pereira, M.F., Castro, A., Chichorro, M., Fernández, C., Diaz-Alvarado, J., Martí, J. and Rodriguez, C.:
827 Chronological link between deep-seated processes in magma chambers and eruptions: Permo-
828 Carboniferous magmatism in the core of Pangea (Southern Pyrenees). *Gondwana Research* 25, 290-308,
829 2014b.

830

831 Pereira, M.F., Chichorro, M., Johnston, S., Gutiérrez-Alonso, G., Silva, J., Linnemann, U., Hofmann, M.
832 and Drost, K.: The missing Rheic ocean magmatic arcs: provenance analysis of Late Paleozoic
833 sedimentary clastic rocks of SW Iberia. *Gondwana Research* 22, 882-891, 2012a.

834

835 Pereira, M.F., Chichorro, M., Silva, J., Ordóñez-Casado, B., Lee, J. and Williams, I.: Early Carboniferous
836 wrenching, exhumation of high-grade metamorphic rocks and basin instability in SW Iberia; constrains
837 derived from structural geology and U–Pb and ⁴⁰Ar-³⁹Ar geochronology. *Tectonophysics* 558-559, 28-
838 44, 2012b.

839

840 Pereira, M.F., Solá, A.R., Chichorro, M., Lopes, L., Gerdes, A. and Silva, J.B.: North-Gondwana
841 assembly, break-up and paleogeography: U-Pb isotope evidence from detrital and igneous zircons of
842 Ediacaran and Cambrian rocks of SW Iberia. *Gondwana Research* 22(3-4): 866-881, 2012c.

843

844 Pereira, M.F., Silva, J.B., Drost, K., Chichorro, M. and Apraiz, A.: Relative timing of transcurrent
845 displacements in northern Gondwana: New U-Pb laser ablation MS-ICP-MS zircon and monazite
846 geochronology of gneisses and sheared granites from the Western Iberian Massif (Portugal). *Gondwana*
847 *Research* 17 (2-3), 461-481, 2010.

848

849 Pereira, M.F., Chichorro, M., Williams, I.S., Silva, J.B., Fernandez, C., Diaz-Azpiroz, M., Apraiz, A. and
850 Castro, A.: Variscan intra-orogenic extensional tectonics in the Ossa-Morena Zone (Évora-Aracena-Lora
851 del Rio metamorphic belt, SW Iberian Massif): SHRIMP zircon U-Th-Pb geochronology. In: Murphy,
852 J.B., Keppie, J.D., Hynes, A.J. (Eds.), *Ancient Orogens and Modern Analogues* Geological Society,
853 London, Special Publications 327, 215-237, 2009.

854

855 Pereira, M.F., Chichorro, M., Williams, I.S. and Silva, J.B.: Zircon U-Pb geochronology of paragneisses
856 and biotite granites from the SW Iberia Massif. (Portugal): evidence for a paleogeographic link between
857 the Ossa-Morena Ediacaran basins and the West African craton. In: Ennih, N., Liégeois, J.P. (Eds.), *The*
858 *Boundaries of the West African Craton*. Geological Society Special Publication, London 297, 385-408,
859 2008.

860

861 Pereira, M.F., Silva, J.B., Chichorro, M., Moita, P., Santos, J.F., Apraiz, A. and Ribeiro, C.: Crustal
862 growth and deformational processes in the Northern Gondwana margin: constraints from the Évora

863 Massif (Ossa-Morena Zone, SW Iberia, Portugal). In: Linnemann, U., Nance, R.D., Kraft, P., Zulauf, G.
864 (Eds.), *The evolution of the Rheic Ocean: from Avalonian–Cadomian active margin to Alleghenian-*
865 *Variscan Collision Special Paper of the Geological Society of America* 423, 333-358, 2007.
866
867 Pereira, M.F., Chichorro, M., Linnemann, U., Eguiluz, L. and Silva, J.B.: Inherited arc signature in
868 Ediacaran and Early Cambrian basins of the Ossa-Morena Zone (Iberian Massif, Portugal):
869 Paleogeographic link with European and North African correlatives. *Precambrian Research* 144, 297-315,
870 2006.
871
872 Pérez-Cáceres, I., Poyatos, D.M., Simancas, J.F. and Azor, A.: Testing the Avalonian affinity of the South
873 Portuguese Zone and the Neoproterozoic evolution of SW Iberia through detrital zircon populations.
874 *Gondwana Research* 42, 177-192, 2017.
875
876 Pérez-Cáceres, I., Martínez Poyatos, D., Simancas, J.F. and Azor, A.: The elusive nature of the Rheic
877 Ocean suture in SW Iberia, *Tectonics*, 34, 2429-2450, 2015a.
878
879 Pérez-Cáceres, I., Simancas, J.F., Martínez Poyatos, D., Azor, A. and González Lodeiro, F.: Oblique
880 collision and deformation partitioning in the SW Iberian Variscides. *Solid Earth Discussions*. 7, 3773-
881 3815, 2015b.
882
883 Pin, Ch., Fonseca, P.E., Paquette, J.L., Castro, P. and Matte, Ph.: The ca. 350 Ma Beja igneous complex:
884 a record of transcurrent slab break-off in the southern Iberia Variscan Belt? *Tectonophysics* 461, 356-377,
885 2008.
886
887 Priem, H.N.A., Boelrijk, N.A.I.M., Hebeda, E.H. and Schermerhorn, L.J.G.: Isotopic ages of the
888 Alcáçovas orthogneiss and the Beja porphyries, South Portugal. *Comunicações Serviços Geológicos*
889 *Portugal* 72: 3-7, 1986.
890
891 Quesada, C. and Oliveira, J.T.: *The Geology of Iberia: A Geodynamic Approach. Volume 2: The*
892 *Variscan Cycle* (Simas, F., volume coordinator). *Regional Geology Reviews*, Springer, p. 1-542, 2019.
893
894 Quesada, C., Fonseca, P.E., Munha, J., Oliveira, J.T. and Ribeiro, A.: The Beja–Acebuches Ophiolite
895 (Southern Iberia Variscan fold belt): geological characterization and significance. *Boletín Geológico y*
896 *Minero* 105, 3-49, 1994.
897
898 Quesada, C., Robardet, M. and Gabaldon, V.: Ossa-Morena Zone. Stratigraphy. Synorogenic phase
899 (Upper Devonian–Carboniferous–Lower Permian). In: Dallmeyer, R.D., Martínez García, E. (Eds.), *Pre-*
900 *Mesozoic Geology of Iberia*. Springer-Verlag, Berlin-Heidelberg, 273-279, 1990.
901

902 Ribeiro, A., Munhá, J., Dias, R., Mateus, A., Pereira, E., Ribeiro, L., Fonseca, P., Araújo, A., Oliveira, T.,
903 Romão, J., Chaminé, H., Coke, C. and Pedro, J.: Geodynamic evolution of the SW Europe Variscides.
904 *Tectonics* 26, TC6009, <https://doi.org/10.1029/2006TC002058>, 2007.

905

906 Rodrigues, B., Chew, D.M., Jorge, R.C.G.S., Fernandes, P., Veiga-Pires, C. and Oliveira, J.T.: Detrital
907 zircon geochronology of the Carboniferous Baixo Alentejo Flysch Group (South Portugal); constraints on
908 the provenance and geodynamic evolution of the South Portuguese Zone. *Journal of the Geological*
909 *Society of London*, <http://dx.doi.org/10.1144/jgs2013-084>, 2014.

910

911 Rosas, F.M., Marques, F.O., Balleve, M. and Tassinari, C.: Geodynamic evolution of the SW Variscides:
912 orogenic collapse shown by new tectonometamorphic and isotopic data from western Ossa-Morena Zone,
913 SW Iberia. *Tectonics* 27, TC0080. <https://doi.org/10.1029/2008TC002333>, 2008.

914

915 Santos, J., Mata, J., Gonçalves, F. and Munhá, J.: Contribuição para o conhecimento Geológico-
916 Petroológico da Região de Santa Susana: O Complexo Vulcano-sedimentar da Toca da Moura.
917 *Comunicações dos Serviços Geológicos de Portugal* 73 (1-2), 29-48, 1987.

918

919 Santos, J.F., Andrade, A.S. and Munhá, J.: Magmatismo orogénico Varisco no limite meridional da Zona
920 de Ossa-Morena. *Comunicações dos Serviços Geológicos de Portugal*, 76, 91-124, 1990.

921

922 Sengör, A.M.C., Özeren, S., Zor, E. and Genç, T.: East Anatolian high plateau as a mantle-supported, N-S
923 shortened domal structure: *Geophysical Research Letters*, v. 30, no. 24, p. 8045, 2003.

924

925 Simancas, J.F., Tahiri, A., Azor, A., González Lodeiro, F., Martínez Poyatos, D. and El Hadi, H.: The
926 tectonic frame of the Variscan-Alleghanian orogen in southern Europe and northern Africa.
927 *Tectonophysics* 398, 181-198, 2005.

928

929 Simancas, J.F., Carbonell, R., González Lodeiro, F., Pérez Estaún, A., Juhlin, C., Ayarza, P., Kashubin,
930 A., Azor, A., Martínez Poyatos, D., Sáez, R., Almodóvar, G.R., Pascual, E., Flecha, I. and Martí, D.:
931 Transpressional collision tectonics and mantle plume dynamics: the Variscides of southwestern Iberia.
932 *Geological Society of London Memoirs*, 32, 345-354, 2006

933

934 Simancas, J.F., Azor, A., Martínez Poyatos, D.J., Tahiri, A., El Hadi, H., González-Lodeiro, F., Pérez-
935 Estaún, A. and Carbonell, R.: Tectonic relationships of Southwest Iberia with the allochthons of
936 Northwest Iberia and the Moroccan Variscides. *Compte Rendus Geoscience* 341, 103-113, 2009.

937

938 Spencer, C.J., Kirkland, C.L., and Taylor, R.J.M.: Strategies towards statistically robust interpretations of
939 in situ U-Pb zircon geochronology. *Geoscience Frontiers* 7, 581-589, 2015.

940

941 Stampfli, G.M., von Raumer, J. and Borel, G.D.: The Palaeozoic evolution of pre-Variscan terranes: from
942 peri-Gondwana to the Variscan collision. In: Martinez-Catalan, J.R., Hatcher, R.D., Arenas, R., Diaz
943 Garcia, F. (Eds.), *Variscan Appalachian Dynamics: The Building of the Upper Paleozoic Basement*.
944 Geological Society of America Special Paper, 364, 263-280, 2002.

945

946 Stampfli, G.M., Hochard, C., V  rard, C., Wilhem, C. and von Raumer, J.: The formation of Pangea.
947 *Tectonophysics* 593, 1-19, 2013.

948

949 Stampfli, G.M. and Kozur, H.W.: Europe from the Variscan to the Alpine Cycles. In: Gee, D.G.,
950 Stephenson, R.A. (Eds.), *European Lithosphere Dynamics*. Geological Society of London Memoirs 32,
951 57-82, 2006.

952

953 Teixeira, C.: Sobre a flora fossil do Carb  nico alentejano. *Boletim do Museu do Laborat  rio de geologia,*
954 *Universidade de Lisboa, 3   s  rie, 7-8: 83-100, 1938-1940.*

955

956 Teixeira, C.: Sur quelques insectes fossiles du Carbonifere de l'Alentejo. *Anais Faculdade de Ci  ncias,*
957 *Porto, vol. XXVI, 2: 117-120, 1941.*

958

959 Teixeira, C.: O Antracol  tico continental portugu  s. (Estratigrafia- Tect  nica). *Boletim da Sociedade*
960 *Geol  gica, porto, vol. 5, Fasc.1-2: 1-139, 1944.*

961

962 Torsvik, T.H., Van der Voo, R., Preeden, U., Mac Niocaill, C., Steinberger, B., Doubrovine, P.V., van
963 Hinsbergen, D.J.J., Domeier, M., Gaina, C., Tohve, E., Meert, J.G., McCausland, P.J.A. and Cocks, R.M.:
964 Phanerozoic polar wander, paleogeography and dynamics. *Earth-Science Reviews* 114, 325-368, 2012.

965

966 Vermeesch, P.: Multi-sample comparison of detrital age distributions. *Chemical Geology* 341, 140-146,
967 2013.

968

969 Vermeesch, P.: IsoplotR: A free and open toolbox for geochronology. *Geoscience Frontiers* 9, 5, 1479-
970 1493, 2018

971

972 von Raumer, J.F., Nesbor, H.-D. and Stampfli, G.M.: The north-subducting Rheic Ocean during the
973 Devonian: consequences for the Rhenohercynian ore sites. *International Journal of Earth Sciences*
974 *(Geologische Rundschau)*. <http://dx.doi.org/10.1007/s00531-016-1425-x>, 2016.

975

976 Wagner, R.H. and Lemos de Sousa, M.J.: The Carboniferous megafloras of Portugal-a revision of
977 identifications and discussion of stratigraphic ages. In: Sousa, M.J.L., Oliveira, J.T. (Eds.), *The*
978 *Carboniferous of Portugal*. *Mem  rias dos Servi  os Geol  gicos de Portugal, Lisboa, pp. 127-152, 1983.*

979

980 Wissink G.K., Wilkinson, B.H., and Hoke, G.D: Pairwise sample comparisons and multidimensional
981 scaling of detrital zircon ages with examples from the North American platform, basin, and passive
982 margin settings. *Lithosphere* 10, 3, 478-491, 2018.

983

984 Yamaji, A.: Slab rollback suggested by latest Miocene to Pliocene forearc stress and migration of
985 volcanic front in southern Kyushu, northern Ryukyu Arc. *Tectonophysics* 364, 9-24, 2003.

986

987 **Figure captions**

988 Figure 1: A- Inset with location of SW Iberia in the Iberian Variscan belt with regional
989 distribution of the main Paleozoic terranes: CIZ- Central Iberian Zone; CZ- Cantabrian Zone;
990 GTMZ- Galicia-Trás-os-Montes Zone; OMZ- Ossa-Morena Zone; PLZ- Pulo do Lobo Zone;
991 SPZ- South-Portuguese Zone and WALZ- West Asturian-Leonese Zone. B- Simplified
992 Geological Map of SW Iberia showing the South-Portuguese, Pulo do Lobo and Ossa-Morena
993 zones (Modified from Pereira et al. 2017a, 2019 and references therein; Quesada and Oliveira,
994 2019).

995

996 Figure 2: Simplified geological map and schematic stratigraphy of the Santa Susana-São
997 Cristovão region (Ossa-Morena Zone; Modified from Gonçalves and Carvalhosa, 1984;
998 Machado et al., 2012). Sampling locations of the Carboniferous sedimentary and igneous rocks
999 used for geochronology are indicated with yellow stars.

1000

1001 Figure 3: Photographs of the Carboniferous igneous rocks of the Santa Susana-São Cristovão
1002 region: A- Baleizão porphyry intrusive contact (yellow arrow) with siliciclastic rocks of the
1003 Toca da Moura volcano-sedimentary complex; B- Baleizão porphyry; C-D- Rhyolitic tuffs of
1004 the Toca da Moura volcano-sedimentary complex; E- Volcanic breccia with fragments of
1005 siltstone (black) and rhyolite (yellow) at the base of the silicic tuffs from the Toca da Moura
1006 volcano-sedimentary complex; F- Silicic volcanic rock interbedded with siltstones of the
1007 Cabrela volcano-sedimentary complex.

1008

1009 Figure 4: Photographs of the Carboniferous sedimentary rocks of the Santa Susana Formation
1010 lower member: A- View of dipping meter-thick beds of medium-coarse grained sandstone
1011 intercalated with conglomerate; B- Planar-bedded coarse-grained sandstone; C- Plant imprints
1012 in sandstone; D- Conglomerate with cobbles and pebbles of granite (G), quartzite (Q), silicic
1013 porphyry (SP) and mafic volcanic rock (M); E- Conglomerate with pebbles of rhyolite (R),
1014 phyllite (P), felsic tuff (T) and quartzite (Q).

1015

1016 Figure 5: Petrographic images of the Carboniferous sedimentary and igneous rocks of the Santa
1017 Susana-São Cristovão region: A- Rhyolitic-rhyodacitic tuff of the Toca da Moura volcano-
1018 sedimentary complex showing quartz and feldspar phenocrysts enclosed in ash matrix; B-
1019 Rhyolitic tuff showing flattened dark-brown millimeter-sized pumice and lithoclasts enclosed in
1020 ash matrix; C- Porphyritic texture of the Baleizão rhyodacite-rhyolite characterized by quartz,
1021 plagioclase, K-feldspar, biotite and amphibole phenocryst embedded in a fine-grained silicic
1022 matrix; D- Cobble of fine-grained granite showing graphic intergrowths of quartz and alkali
1023 feldspar, found in conglomerate from the Santa Susana Formation; E- Siltstone of the Toca da
1024 Moura volcano-sedimentary complex mostly composed of quartz grains and a few grains of
1025 plagioclase (P), tourmaline (T), and rock fragments (L); F- Siltstone of the Cabrela volcano-
1026 sedimentary complex showing fining upwards grading and a slump-fold; G-H, Sandstones from
1027 the Santa Susana Formation with high percentage of lithoclasts (L) and a few feldspar (F).

1028

1029 Figure 6: Concordia diagrams, weighted mean of $^{206}\text{Pb}/^{238}\text{U}$ ages of analyzed zircon grains
1030 extracted from silicic volcanic rocks of the Toca da Moura and Cabrela volcano-sedimentary
1031 complex.

1032

1033 Figure 7: Concordia diagrams, weighted mean of $^{206}\text{Pb}/^{238}\text{U}$ ages of analyzed zircon grains of:
1034 A- the Baleizão porphyry and B- the cobble of granite found in conglomerate from the Santa
1035 Susana Formation.

1036

1037 Figure 8: Pie diagrams and Kernel Density Estimation (KDE) with U-Pb detrital-zircon ages of
1038 siliciclastic rocks from: A- the Toca da Moura (TM-3, this study) and Cabrela (CB: CBR-11,
1039 this study; and OM-200, Pereira et al., 2012a) volcano-sedimentary complexes, and B- the Santa
1040 Susana Formation (SS-1 and SS-2, this study; and SS Upper member, StSz2 and StSz4 from
1041 Dinis et al., 2018); C- U-Pb age cumulative frequency plots applied to the U-Pb ages (90-110%
1042 concordance) of detrital zircon grains from the Toca da Moura and Cabrela volcano-
1043 sedimentary complexes, and the Santa Susana Formation.

1044

1045 Figure 9: Multi-Dimensional Scaling diagrams (Vermeesch, 2018) applied to the U-Pb ages (90-
1046 110% concordance) of detrital zircon grains from the Toca da Moura (TM-3) and Cabrela (CB)
1047 volcano-sedimentary complexes, and the Santa Susana Formation (SS1, SS2, SS upper
1048 member), and different potential sources: OMZ (Linnemann et al. 2008; Pereira et al. 2008,
1049 2012c), PLZ (Pereira et al. 2017a; Pérez Cáceres et al. 2017), SPZ (Braid et al. 2011; Pereira et
1050 al., 2012a, 2014a; Rodrigues et al. 2014). Abbreviations: MT- Mértola Formation; MR- Mira
1051 formation; BJ- Brejeira formation; PQ-TRC- Phyllite-Quartzite and Tercenas formations; SI-

1052 REP- Santa Iria and Represa formations; P-G-R-A-R- Pulo do Lobo, Gafo, Ribeira de Lima,
1053 Atalaia and Ronquillo formations; HT- Horta da Torre Formation.
1054
1055 Figure 10: Sketches showing inferred tectonic evolution and sedimentation recorded in SW
1056 Iberia Carboniferous stratigraphy during Laurussian-Gondwana oblique collision (Modified
1057 from Pereira et al., 2012b; 2020); A- Late Devonian; B1-B2- Early Carboniferous; C1-C2- Late
1058 Carboniferous.
1059

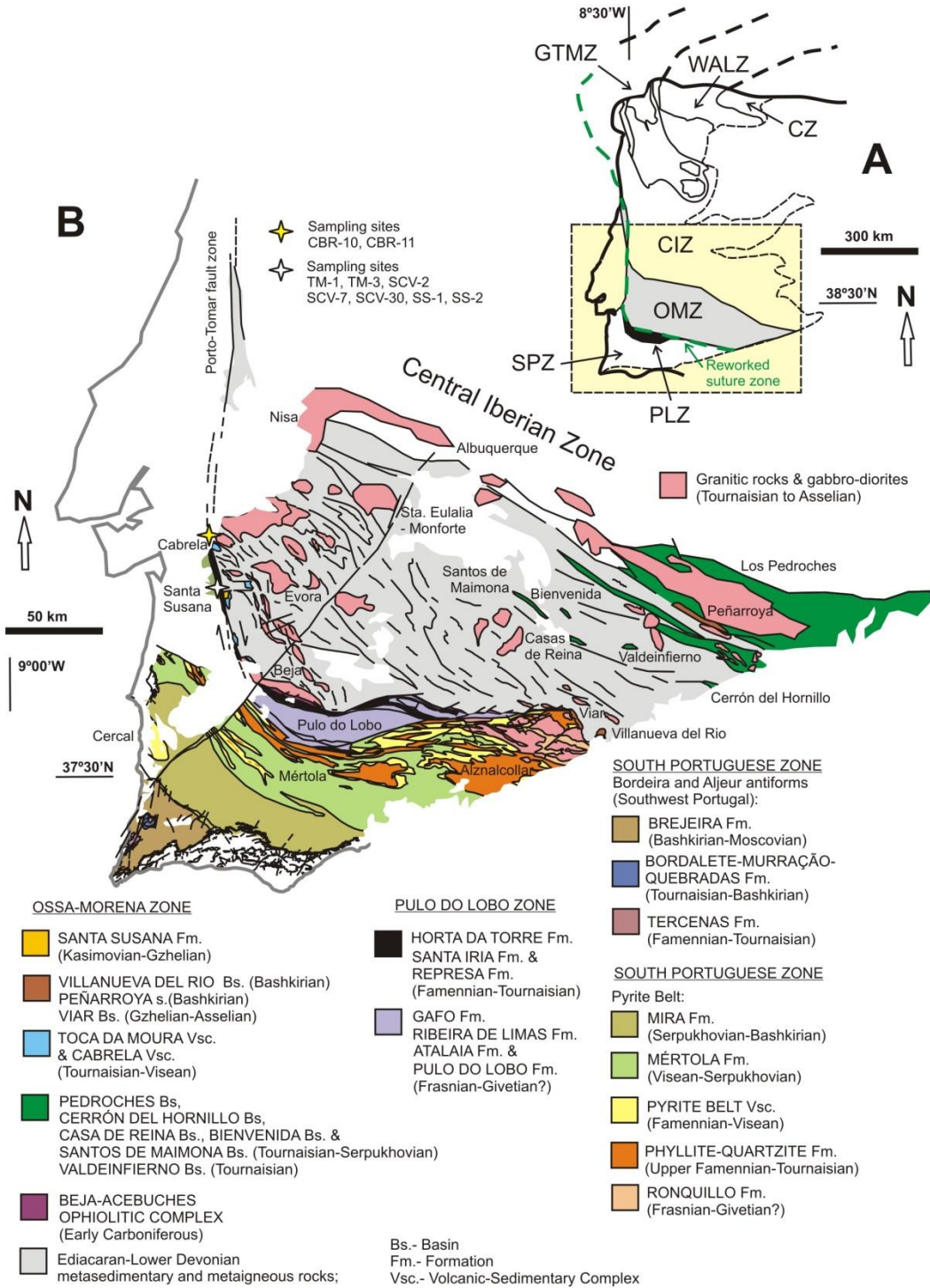


Figure 1

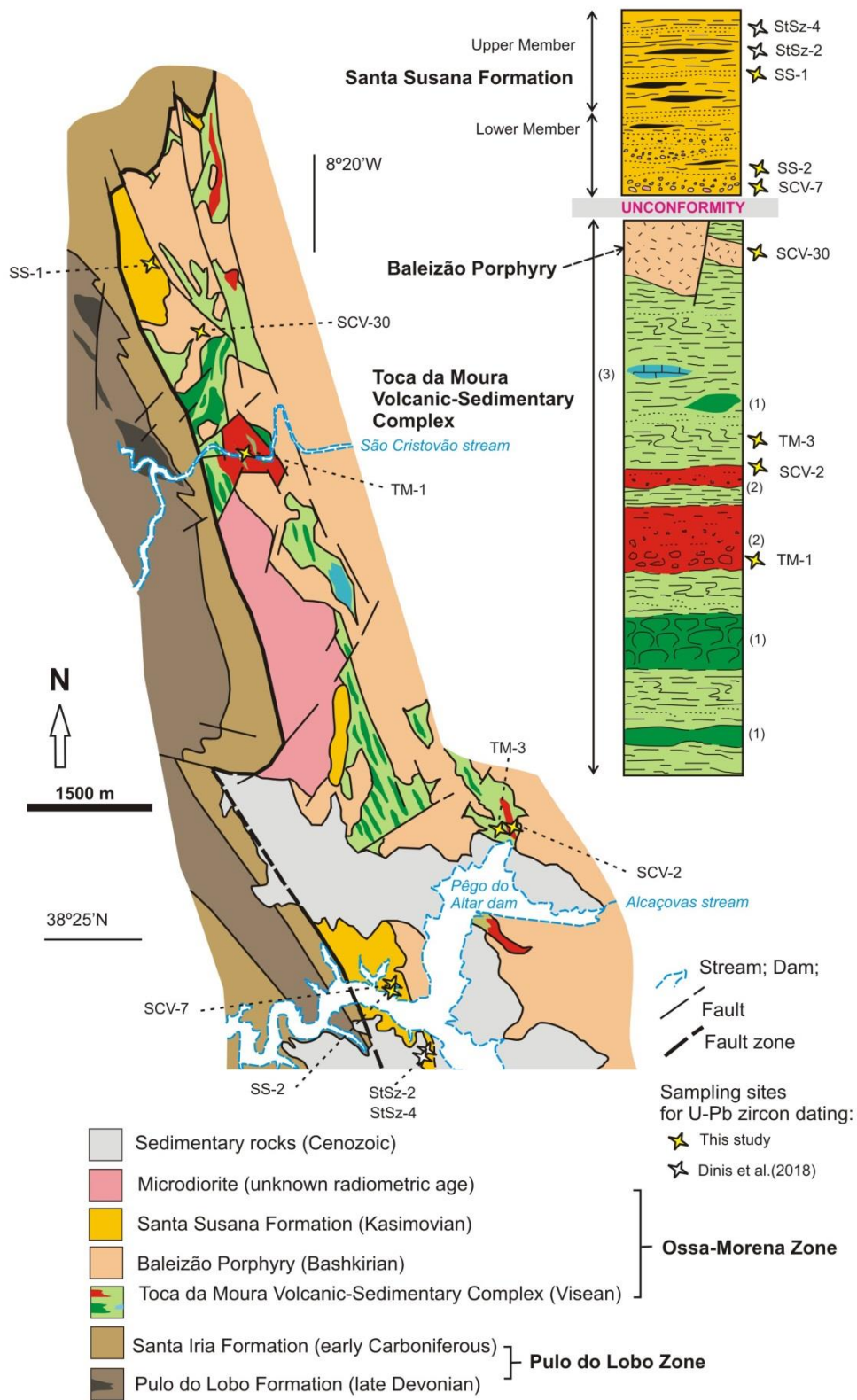


Figure 2

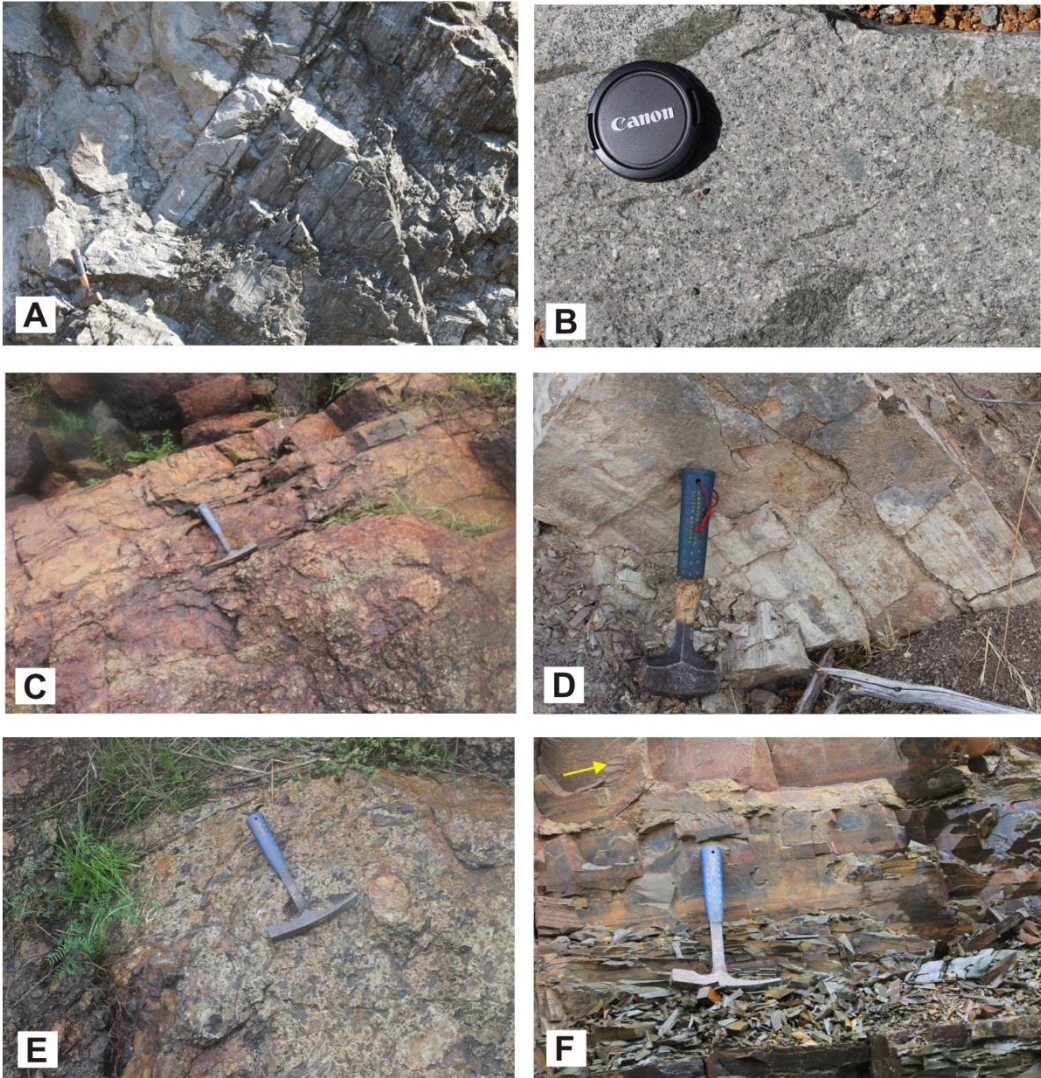


Figure 3

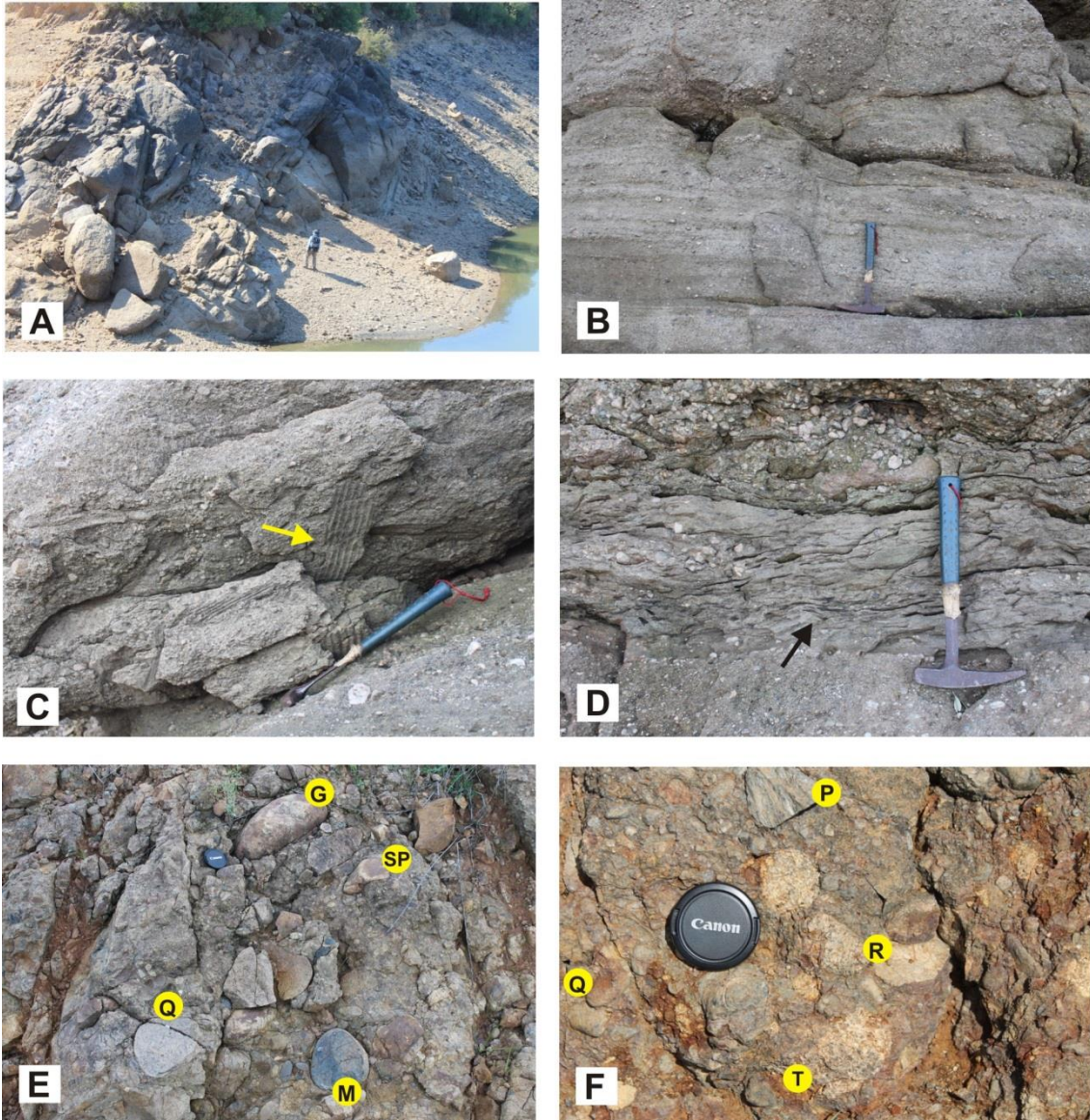


Figure 4

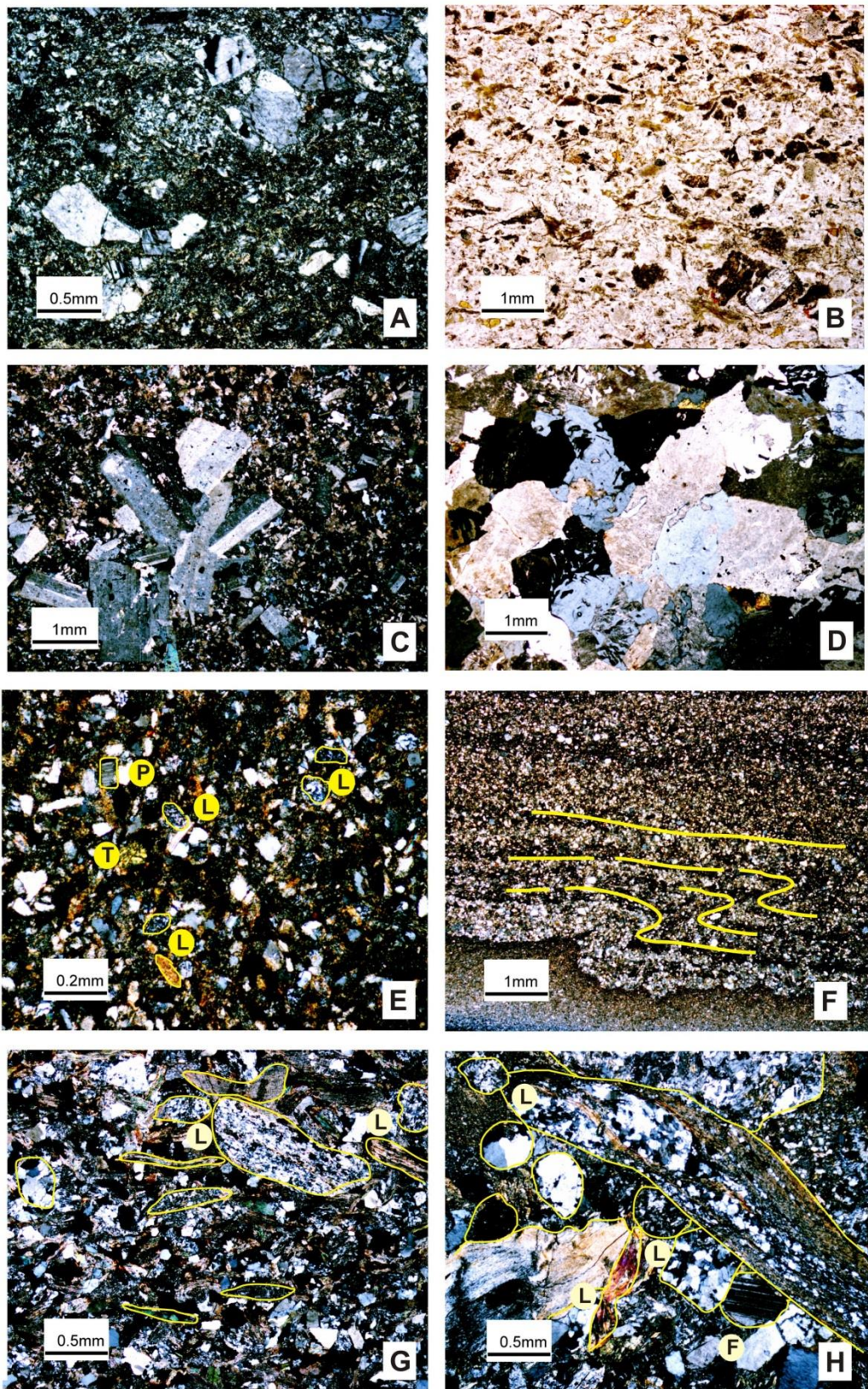


Figure 5

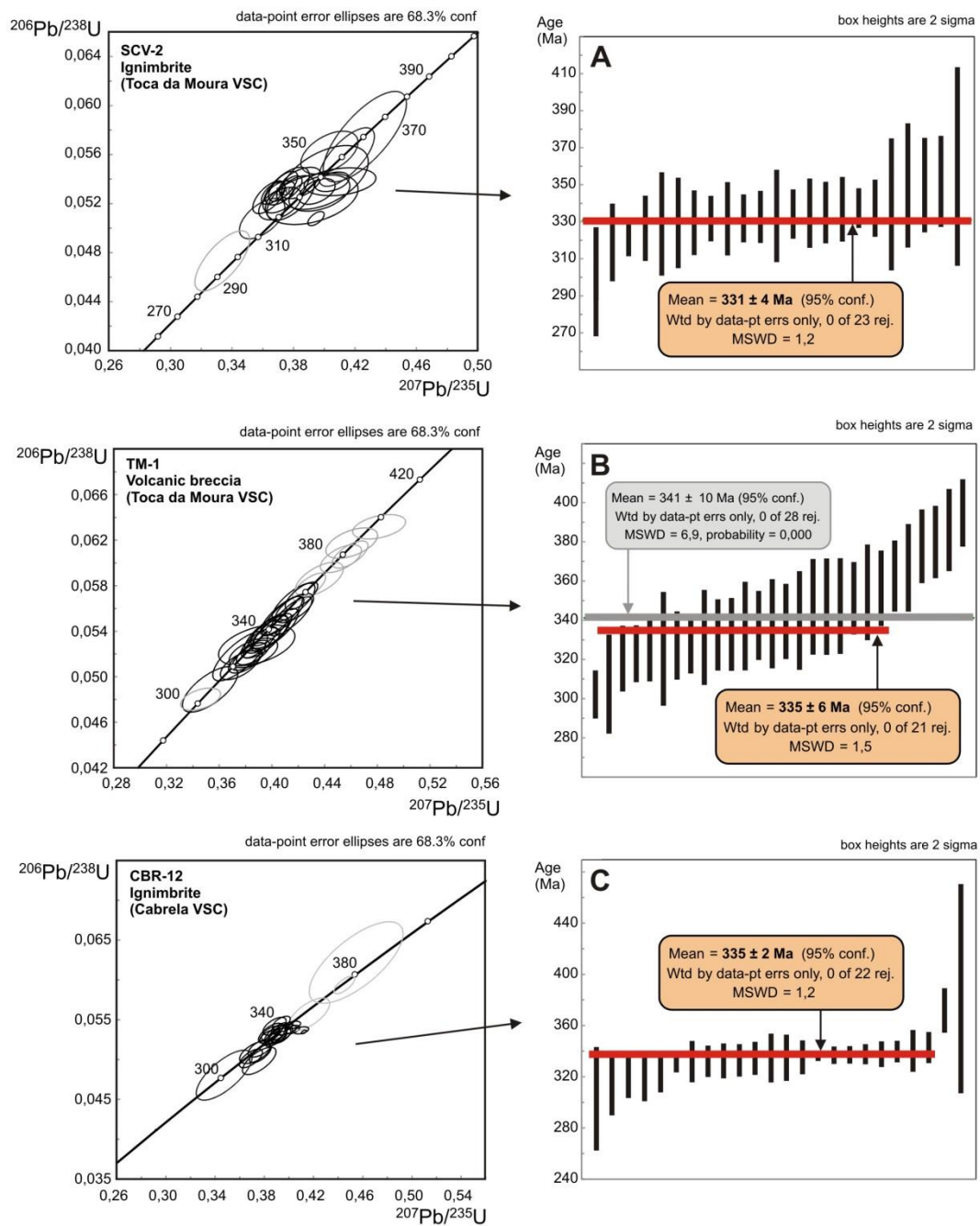


Figure 6

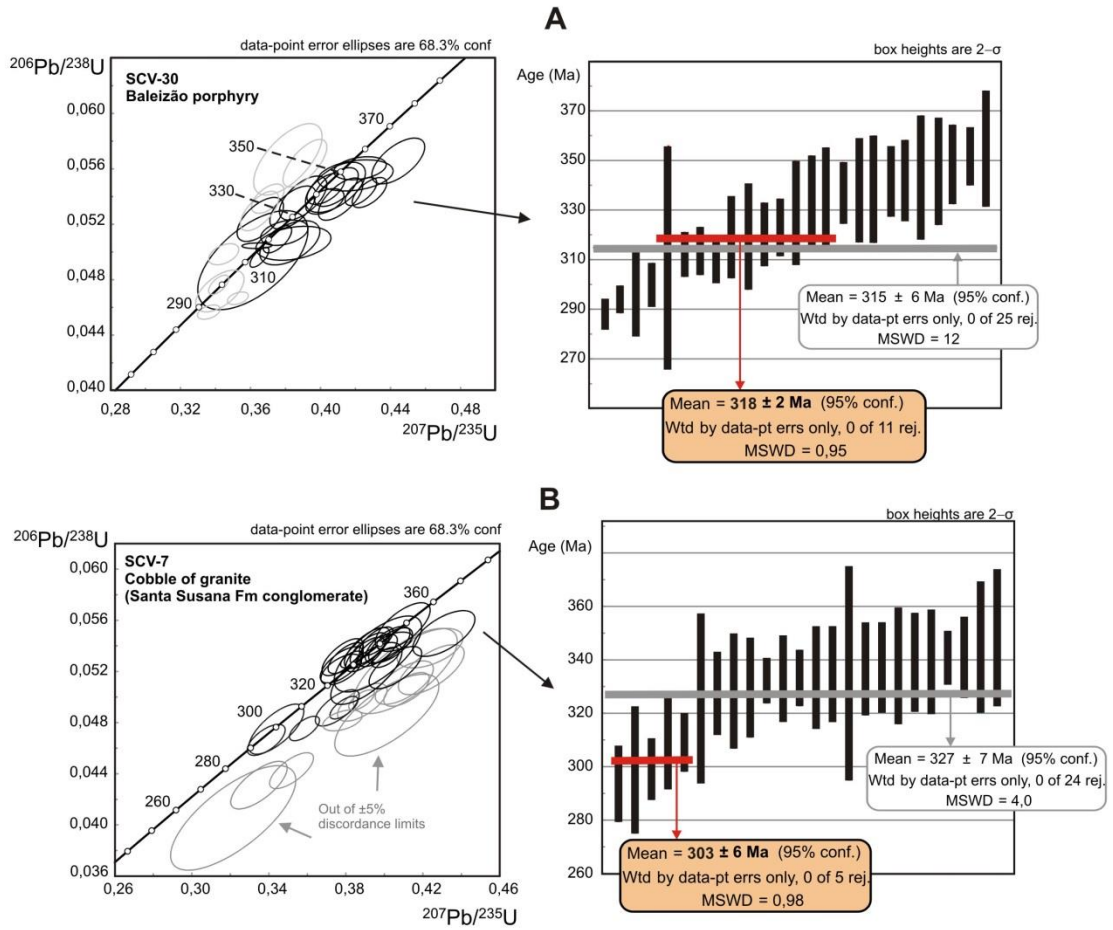


Figure 7

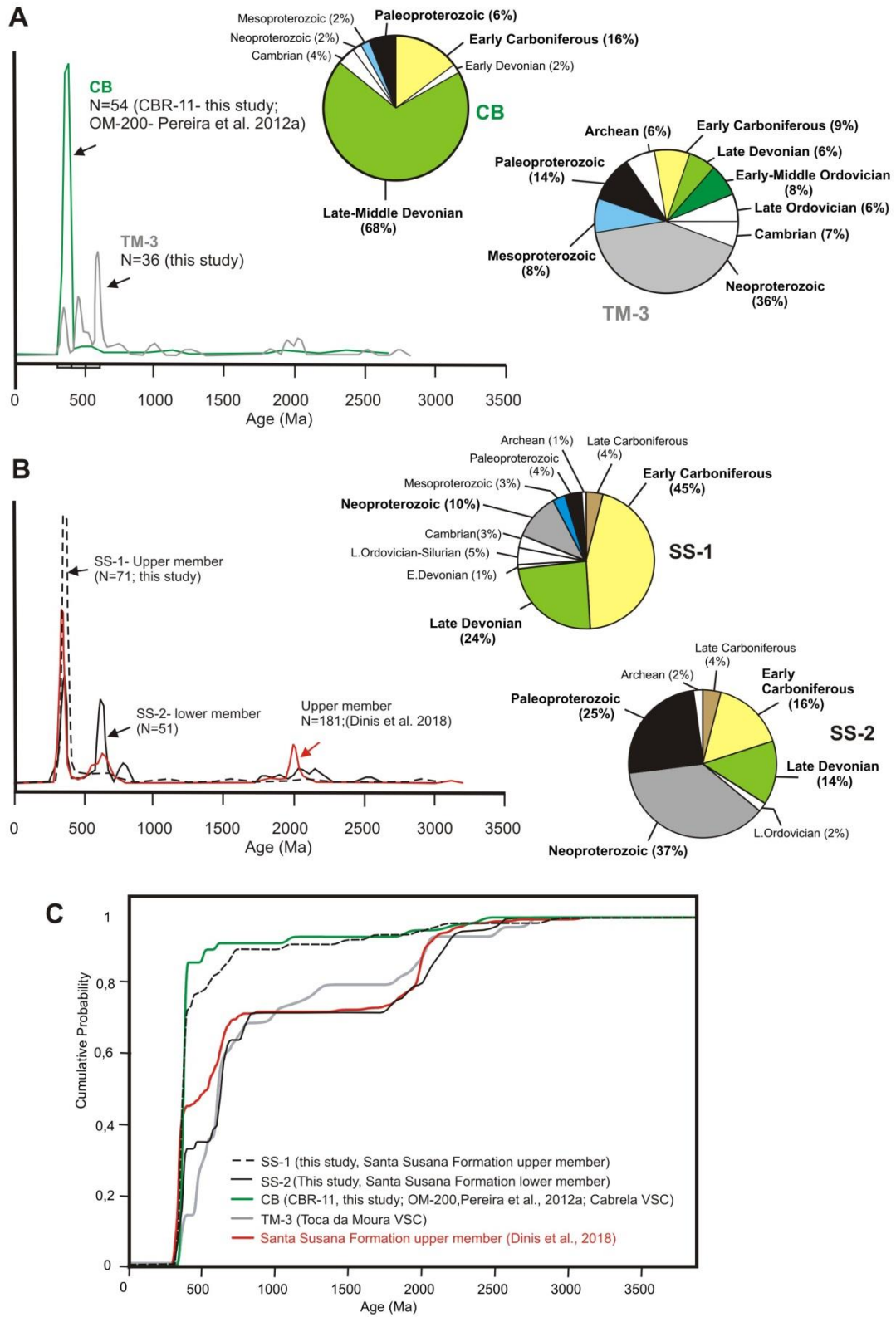


Figure 8

MDS diagrams

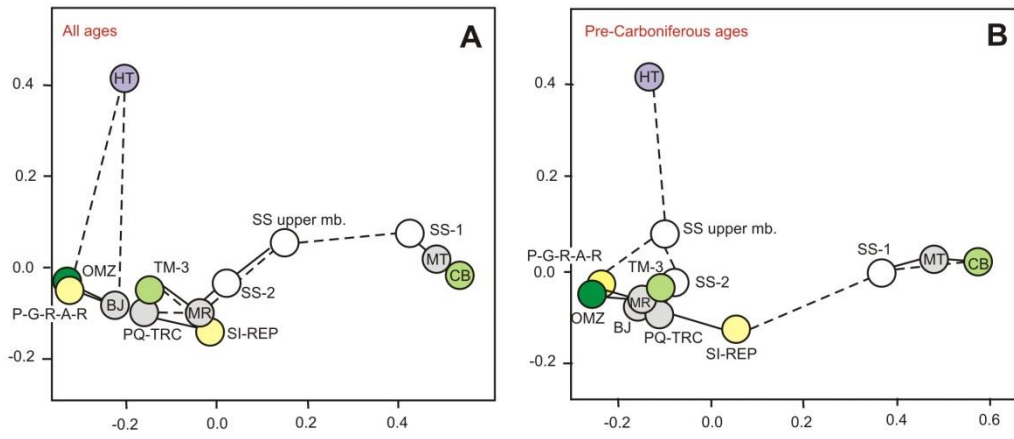


Figure 9

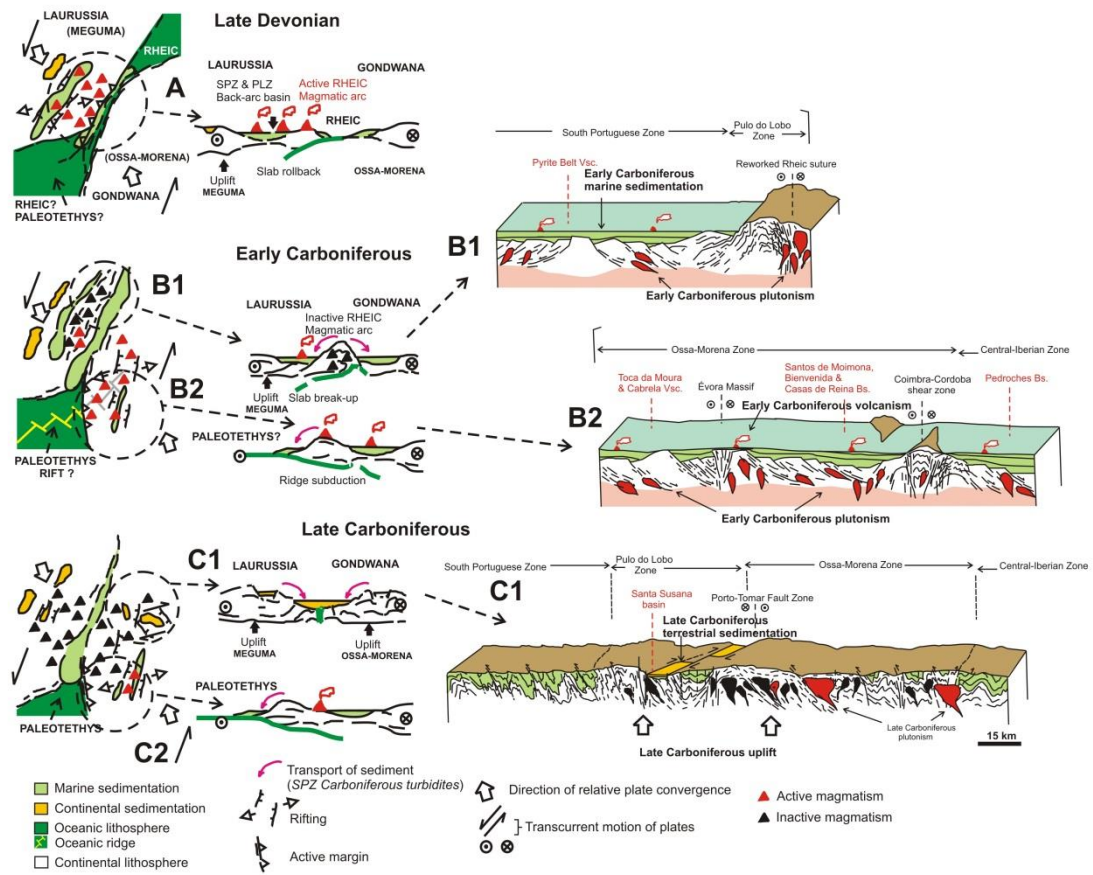


Figure 10